THE AMERICAN MINERALOGIST, VOL. 49, JULY–AUGUST, 1964

CELADONITE: SYNTHESIS, THERMAL STABILITY AND OCCURRENCE[1]

W. S. WISE[2] AND H. P. EUGSTER, *Department of Geology, The Johns Hopkins University, Baltimore, Maryland.*

ABSTRACT

Celadonite, a blue-green clay mineral with the structure of dioctahedral micas, is widespread in formations of altered volcanic rocks of intermediate to basaltic composition. It occurs throughout the zeolite and prehnite-pumpellyite facies but does not occur in the greenschist facies.

Six end members can be used to express the chemical compositions of celadonites; of these $KMgFe^{3+}Si_4O_{10}(OH)_2$ is the most important. Glauconite apparently differs from celadonite in the amount of Al substituted in the tetrahedral positions. All celadonites investigated are the 1M polymorph.

The $MgFe^{3+}$-celadonite was synthesized, and its stability studied with oxygen buffer techniques. The upper stability limit is near 410° C., varying only slightly with changes in oxygen fugacity or total pressure. The $MgFe^{+3}$-celadonite breaks down to ferri-biotite, ferri-sanidine, and quartz at high f_{O_2} conditions and to ferri-biotite, quartz, and liquid at low f_{O_2} conditions. New data on the stability of ferri-sanidine elucidate phase relations at higher temperatures. Attempts to synthesize the other celadonite end members have been largely unsuccessful, except for the $Fe^{2+}Fe^{3+}$-celadonite.

Celadonite in metamorphosed volcanic rocks seems to disappear long before its upper stability limit is reached. Of several explanations considered, reactions with hydrous aluminum silicates (usually clays, such as montmorillonite) probably account for the lack of celadonite in greenschist facies rocks. An extended μ_{H_2O}-μ_{CO_2} diagram, to indicate a possible series of reactions through the zeolite facies, seems to suggest that special bulk compositions are necessary for celadonite to be preserved at higher grades of metamorphism.

INTRODUCTION

Celadonite is a blue-green, earthy to micaceous mineral. It is a common constituent of altered basic and intermediate volcanic sediments and lavas. It has a mica lattice and ideally is dioctahedral and tetrasilicic, with compositions near $K(Mg,Fe^{2+})(Al,Fe^{3+})Si_4O_{10}(OH)_2$. All celadonites investigated so far are of the 1M type (Yoder and Eugster, 1955).

The name "celadonite," derived from the French word, *celadon*, meaning sea green, was proposed by Glocker (1847) for a soft pale green mineral that was found to be a hydrous potassium, magnesium, iron silicate. In a paper describing the occurrences of celadonite in Scotland, Heddle (1879) suggested that similar material was earlier described by DeLisle (1783), who named it *terra verdi* and also by Hofmann (1788), who used the name *Grünerde*.

The similar chemical nature of celadonites and glauconites was recog-

[1] Work supported by a grant from the National Science Foundation.

[2] Present address: University of California at Santa Barbara, Santa Barbara, California.

nized early. During a study of the occurrences and chemical and x-ray characteristics of glauconites and celadonites, Hendricks and Ross (1941, p. 708) came to the following conclusion:

"As the well established term 'glauconite' is used for a mineral of characteristic sedimentary origin whereas the term 'celadonite' is used for a mineral of quite a different occurrence and paragenesis, it seems best to retain both names."

Recent studies by Coombs (1954), Fiske (1960), and Wise (1961) show that celadonite is an important mineral in altered volcanic clastic rocks. It was found to be present in many assemblages of the zeolite facies, but does not seem to extend to assemblages of the greenschist facies.

Acknowledgments

The work was carried out at The Johns Hopkins University, and part of it was reported in a Ph.D. dissertation submitted there (Wise, 1961). The research was supported by a grant from the National Science Foundation. D. S. Coombs, D. R. Wones and A. C. Waters critically read the manuscript, and their comments have led to its improvement; however, they should not be considered committed to the writers' views.

Natural Celadonites

Chemical composition. From the chemical compositions of celadonites and glauconites a layered structure was proposed by early workers, but Gruner (1935) was the first to show that these minerals have the mica structure. Gruner indexed the reflections of a glauconite x-ray powder pattern and compared it to that of biotite. The similarity to mica patterns was later verified by Maegdefrau and Hoffman (1937) and by Hendricks and Ross (1941). Yoder and Eugster (1955) pointed out that a natural celadonite from Reno, Nevada is of the 1M type, and recent work on the chemistry of micas by Foster (1960) has shown that some natural celadonites lie very close to the ideal tetrasilicic end members.

Figure 1 shows the relationship in crystal chemistry between ideal celadonite and muscovite. The primary difference between the two, as pointed out by Foster (1960), is the origin of the negative layer charge. In celadonite two of the three octahedral positions are filled with one divalent and one trivalent atom. This gives rise to a minus one charge for the octahedral layer, and this charge is neutralized by the interlayer cations. The tetrahedral layers are electrically neutral, since all four positions are occupied by silicon atoms. In the muscovites, which are ideally trisilicic, one of the four silicon atoms is replaced by aluminum; the tetrahedral layers have a minus one charge, which is neutralized by the interlayer cations. Octahedral sites in muscovites are filled with two trivalent atoms, which satisfy the anionic valences, and no charge arises from the octahedral layer.

Compared with glauconite, few occurrences and analyses of celadonites have been reported. Because celadonite in altered tuffs is finely disseminated, amygdule fillings of lavas are the only occurrence in which enough material may be found for chemical analysis. The most recent celadonite analyses have been published by Schüller and Wohlmann (1951), Bayramgil *et al.* (1952), Malkova (1956), Lazarenko (1956), Gogishvili (1959), and Kardymowicz (1960). These analyses together with the ten analyses given by Hendricks and Ross (1941) are assembled

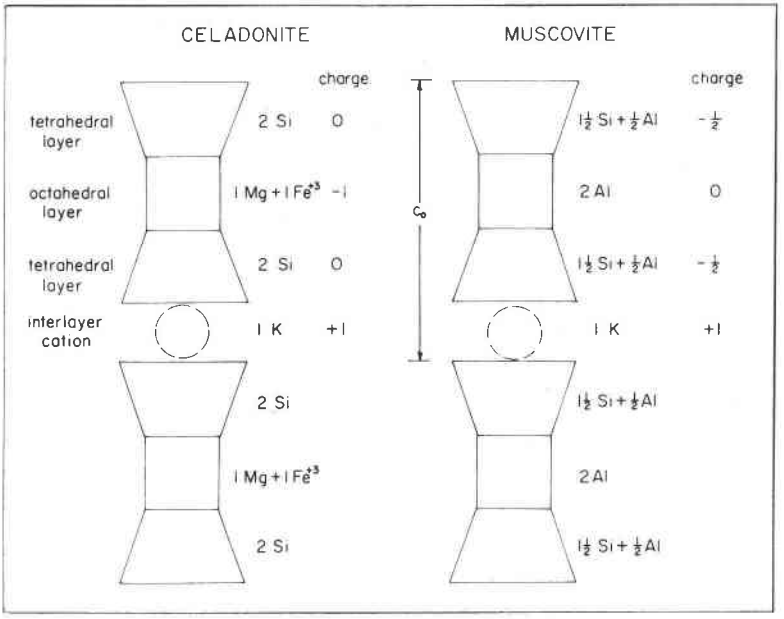

FIG. 1. Schematic representation of the crystal chemistry of celadonite and muscovite, to illustrate the origin of the layer charge.

in Table 1. A new analysis (number 15, Table 1) was made by O. von Knorring, Leeds University, on material from amygdule fillings in the basal part of a basalt flow[1] from southern Washington.

As mentioned by Hendricks and Ross (1941), several of the literature analyses are not reliable because of impurities. The analyses in Table 1

[1] This basalt is interbedded with lower Tertiary volcanic clastic rocks and crops out on Stevenson Ridge near the head waters of Budweiser Creek (sec. 3, T. 3 N., R. 7 E.), Wind River quadrangle, Washington (Wise, 1961). The host rock contains 60% plagioclase phenocrysts and laths, 19% augite, 6% magnetite, and 15% glass and secondary minerals. The celadonite occurs as a cavity filling but also replaces plagioclase phenocrysts (Fig. 6). The refractive indices are: $\gamma = 1.626$, $\alpha = 1.610$, $\gamma - \alpha = 0.016$. The density ranges between 2.95 to 3.05.

TABLE 1. CHEMICAL ANALYSES OF CELADONITES WITH THE AVAILABLE OPTICAL PROPERTIES AND *X*-RAY DATA ($d_{(003)}$ AND $d_{(060)}$)

	1	2	3	4	5	6	7	8	9	10
SiO_2	55.61	53.23	50.6	54.30	54.73	52.69	55.30	50.70	57.72	56.41
TiO_2	—	—	—	—	—	—	—	—	—	—
Al_2O_3	0.79	2.13	4.2	5.08	7.56	5.79	10.90	4.72	0.33	2.14
Fe_2O_3	17.19	20.46	14.1	14.77	13.44	9.75	6.95	15.34	17.05	14.07
FeO	4.02	4.14	3.3	4.82	5.30	5.37	3.54	2.00	3.73	5.10
MgO	7.26	5.67	6.4	6.05	5.76	8.54	6.56	9.32	3.84	5.91
MnO	0.09	—	—	0.09	—	0.31	—	tr	0.08	0.23
CaO	0.21	—	3.1	0.80	0.00	1.16	0.47	1.32	0.60	0.60
Na_2O	0.19	—	0.4	3.82	—	0.39	0.00	0.29	0.42	—
K_2O	10.03	7.95	8.7	4.85	7.40	6.21	9.38	4.44	5.55	8.83
Li_2O	—	—	—	—	—	—	—	—	—	—
H_2O^+, H_2O^-	4.88	6.18	8.3	5.64	6.40	10.48	6.51	12.52	10.78	6.80
CO_2	—	—	—	—	—	—	—	—	—	—
P_2O_5	—	—	—	—	—	—	—	—	—	—
Total	100.27	99.76	99.1	100.22	100.59	100.69	99.61	100.65	100.10	100.09
Classif. of Anal.	A	A	C	A	A	A	B	A	C	C
α	1.610		1.606							
γ	1.641		1.634							
							1.60			
d_{003}	—	—	—	—	—	—	—	—		
$d_{(060)}$	—	—	—	—	—	—	—	—		

	11	12	13	14	15	16	17	18	19
SiO_2	56.47	48.68	52.53	52.58	54.38	56.02	49.85	49.05	49.78
TiO_2	0.13	—	0.25	0.15	0.14	0.43	—	0.21	0.36
Al_2O_3	9.09	—	4.97	6.77	5.41	17.83	4.83	18.17	16.42
Fe_2O_3	12.36	19.44	18.62	20.07	14.22	1.14	20.39	6.42	9.74
FeO	2.19	8.16	4.58	3.33	3.56	2.79	2.49	2.56	3.77
MgO	5.98	5.98	5.35	6.22	6.40	5.21	1.24	—	—
MnO	0.12	—	0.01	tr	0.25	0.03	4.40	3.10	4.71
CaO	1.13	4.35	0.58	0.91	0.42	0.68	1.45	1.03	0.75
Na_2O	0.86	—	0.00	0.05	0.05	—	3.34	0.23	0.15
K_2O	6.49	7.38	7.93	3.33	9.23	9.17	5.80	6.62	7.72
Li_2O	—	—	—	—	0.15	—	—	—	—
H_2O^+, H_2O^-	5.32	3.00	4.31, 1.15	6.75	4.80, 1.16	5.03, 1.51	3.60, 3.23	4.56, 8.91	3.08, 3.60
CO_2	—	2.57	—	—	nd	—	—	—	—
P_2O_5	—	—	—	—	—	0.12	—	—	0.28
Total	100.14	99.56	100.64	100.16	100.17	99.96	100.62	99.86	100.36
Classif. of Anal.	A	C	B	A	A	B	B	A	B
α			1.607		1.610				
γ			1.640		1.633	1.579			1.588

N	1.62	1.620–1.624					1.608		
$d_{(005)}$	3.32	3.312	3.32	3.34	3.318	3.36	—	—	—
$d_{(060)}$	1.50		1.507	1.517	1.509	1.50	—	—	—

Source for analyses:

No.	Reference	Occurrence
1	Wells, 1937 (p. 102)	from vesicular basalt
2	Levi, 1914	
3	Wells, 1937 (p. 102)	from cavities in basalt
4	Lacroix, 1916	
5	Koenig, 1916	
6	Heddle, 1879	amygdules in basalt
7	Maegdefrau and Hofmann, 1937	lavas in Vesuvius
8	Scherillo, 1938	amygdular basalt, pseudomorphs after olivine
9	Heddle, 1879	cavities in basalt
10	Heddle, 1879	druses in basalt
11	Bayramgil, *et al.*, 1952	
12	Schüller and Wohlmann, 1951	
13	Malkova, 1956	veins and vugs in metamorphic rocks
14	Lazarenko, 1956	basalt cavities
15	this paper (analyst: O. von Knorring)	amygdule fillings in basalt
16	Kardymowica, 1960	in tuffite
17	Kvalvaser, 1953	veins in oxykeratophyre
18	Smolikowski, 1936	
19	Gogishvili, 1959	

have been classified, according to standards much like those of Hey (1932). From the analyses of Table 1 structural formulas were calculated by the method of Hendricks and Ross (1941). Values are given in Table 2. Foster (1956, 1960) has used the same method extensively for a variety of micas. In most celadonite analyses only total water is given. Therefore all calculations are based on an assumed content of 12 oxygen and 2 hydrogen atoms per unit cell, that is, a total of 22 cationic charges. As pointed out by Eugster and Wones (1962) and by Foster *et al.* (1963), this procedure is inaccurate with respect to octahedral occupancy for iron-rich micas which contain less than two hydrogen atoms per unit cell. Errors in individual atomic percentages quoted in the structural formulas on Table 2 may be as high as 10%, since a hydrogen free mica would have a total of 24 cationic charges. Values of Table 2 nevertheless are useful for purposes of comparison. Analysis No. 1 represents the only truly tetrasilicic celadonite. The average value for Si in the 17 analyses is 3.83. Except for Nos. 17 to 19 variations are between 3.73 and 4.00. Octahedral occupancy is close to 2 for all celadonites, with an average value of 2.05. Interlayer cations number often substantially less than 1.0 and average at 0.81 with a low value of 0.38 (No. 14). This of course is typical also for glauconites and hydrous micas. Tyler and Bailey (1961) have noticed what appears to be a systematic relationship between octahedral and interlayer occupancy for glauconites.

"Analyses in the literature indicate a well-defined trend towards increase in octahedral cations with decrease in interlayer cations. . . . There is some evidence that for a given interlayer cation content non-marine celadonites tend to have higher octahedral cation totals than do marine glauconites. For the few analyses available of celadonites, however, the scatter of values is too large to enable a definite trend to be plotted."

TABLE 2. STRUCTURAL FORMULAS OF CELADONITES, ASSUMING $O_{10}(OH)_2$

	1	2	3	4	5	6	7	8	9	10
Si	4.00	3.90	3.81	3.86	3.87	3.88	3.88	3.79	4.27	4.09
Al	0.07	0.18	0.37	0.42	0.63	0.50	0.90	0.42	0.03	0.18
Fe^{3+}	0.93	1.13	0.80	0.79	0.71	0.54	0.37	0.86	0.95	0.77
Fe^{2+}	0.24	0.25	0.21	0.29	0.31	0.33	0.21	0.12	0.23	0.31
Mg	0.78	0.62	0.72	0.64	0.61	0.94	0.68	1.04	0.42	0.64
Ca	0.02	—	0.25	0.06	—	0.09	0.04	0.11	0.05	0.05
Na	0.03	—	0.06	0.53	—	0.06	—	0.04	0.06	—
K	0.92	0.74	0.84	0.44	0.67	0.58	0.84	0.42	0.52	0.82
H	1.91	3.02	4.17	2.67	3.02	5.15	3.04	6.24	5.32	3.29
Al^{IV}	—	0.10	0.19	0.14	0.13	0.12	0.12	0.21		
Al^{VI}	0.07	0.08	0.18	0.28	0.50	0.38	0.78	0.21		
ΣOct	2.02	2.08	1.91	2.00	2.13	2.19	2.04	2.23		
Σalk	0.97	0.74	1.15	1.03	0.67	0.73	0.88	0.57		
Ch.T	—	−0.10	−0.19	−0.14	−0.13	−0.12	−0.12	−0.21		
Ch.Oc	−0.96	−0.63	−1.20	−0.93	−0.53	−0.70	−0.77	−0.47		
Ch.alk.	+0.99	+0.74	+1.40	+1.09	+0.67	+0.82	+0.92	+0.68		
ΣCh	+0.03	+0.01	+0.01	+0.02	+0.01	0	+0.03	0		

	11	12	13	14	15	16	17	18	19
Si	3.88	3.56	3.78	3.73	3.90	3.88	3.67	3.61	3.51
Al	0.74	—	0.42	0.57	0.46	1.45	0.42	1.58	1.36
Fe^{3+}	0.64	1.11	1.01	1.07	0.77	0.01	1.13	0.36	0.51
Fe^{2+}	0.13	0.52	0.28	0.20	0.21	0.02	0.15	0.16	0.22
Mg	0.61	0.68	0.57	0.66	0.68[1]	0.54	0.48	0.34	0.50
Ca	0.08	0.36	0.04	0.07	0.03	0.05	0.11	0.08	0.05
Na	0.11	—	—	0.01	0.01	—	0.48	0.03	0.02
K	0.57	0.72	0.73	0.30	0.84	0.81	0.54	0.53	0.70
H	2.44+	1.53	2.07+	3.19	2.30+	2.32	1.77	2.24	1.98
Al^{IV}	0.12	—	0.22	0.27	0.10	0.12	0.33	0.39	0.49
Al^{VI}	0.62	—	0.20	0.30	0.36	1.33	0.09	1.19	0.87
ΣOct	2.00	—	2.06	2.23	2.02	1.90	1.85	2.05	2.10
Σalk	0.76	—	0.77	0.38	0.88	0.86	1.13	0.64	0.77
Ch.T	−0.12	—	−0.22	−0.27	−0.10	−0.12	−0.33	−0.39	−0.49
Ch.Oct.	−0.74	—	−0.67	−0.17	−0.83	−0.86	−1.08	−0.35	−0.42
Ch.alk	+0.84	—	+0.83	+0.45	+0.91	+0.91	+1.24	+0.72	+0.82
ΣCh.	−0.02	—	−0.06	+0.01	−0.02	−0.07	−0.17	−0.02	−0.09

[1] Includes Li_2O.

These conclusions are not well borne out by the data of Table 2. Figure 2, a plot of octahedral vs. interlayer occupancy, indicates a trend for the celadonites very near that for the glauconites of Hendricks and Ross (1941), Owens and Minard (1960), and Burst (1958).

The data of Table 2 are plotted in Figs. 3 and 4 along with similar data from published glauconite analyses, calculated in the same way as the

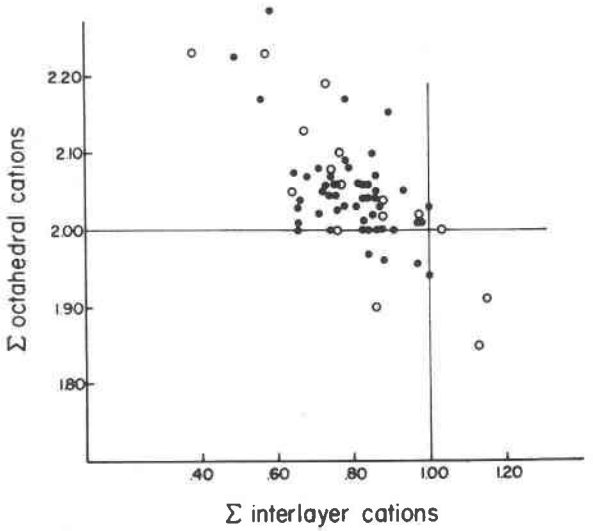

FIG. 2. Plot of the total number of cations in octahedral positions vs. the total number of interlayer cations. Celadonite points are represented by open circles (data from Table 2); glauconites, by closed circles (data from Hendricks and Ross (1941), Burst (1958), and Owens and Minard (1960)).

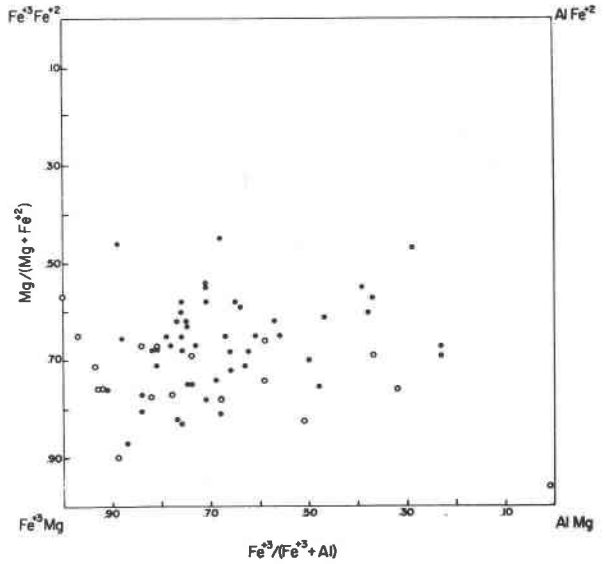

FIG. 3. Plot of the composition of the octahedral layer of celadonites and glauconites, using $Mg/Mg+Fe^{2+}$ and $Fe^{3+}/Fe^{3+}+Al$ ratios. Celadonite points are open circles, and glauconites are closed circles. Sources of data are the same as for Fig. 2.

celadonites (see, for instance, Owens and Minard, 1960). The composition of the octahedral layer is shown in Fig. 3. This plot shows that among the four idealized tetrasilicic end members of celadonite the first is the most important:

$$KMgFe^{3+}Si_4O_{10}(OH)_2 \quad (1)$$

$$KFe^{2+}Fe^{3+}Si_4O_{10}(OH)_2 \quad (2)$$

$$KMgAlSi_4O_{10}(OH)_2 \quad (3)$$

$$KFe^{2+}AlSi_4O_{10}(OH)_2 \quad (4)$$

End member (3) has been called leucophyllite, and analysis No. 16 comes closest to this end member.

In a plot of the compositions of dioctahedral layered silicates, Yoder and Eugster (1955, p. 257) indicate that the amount of trivalent atoms in tetrahedral coordination is a characteristic difference between celadonites and glauconites. Figure 4 is a similar triangular plot to show the variations in the number of silicon atoms in tetrahedral coordination. Celadonites have 4.0 to 3.70 Si in tetrahedral positions, whereas most of the glauconites fall between 3.80 and 3.40. In order to account for this substitution of Al (or Fe^{3+}) for Si in the tetrahedral positions, the compositions of most celadonites and all glauconites must be represented by

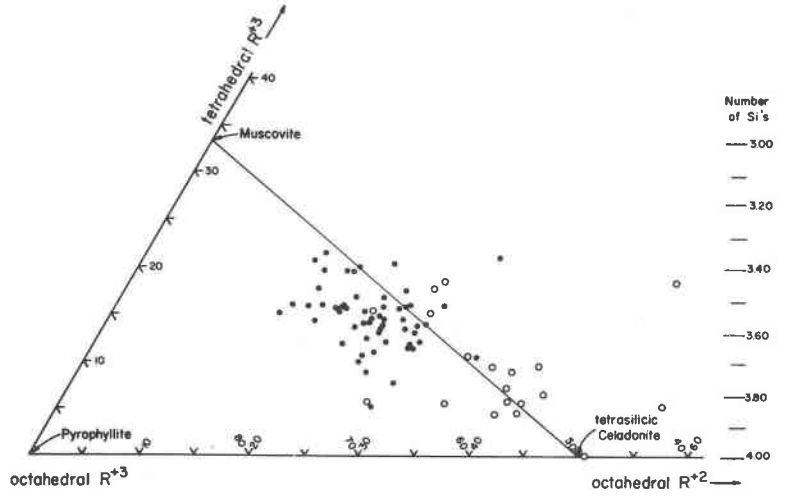

FIG. 4. Triangular plot with total tetrahedral R^{3+} cations, total octahedral R^{3+} cations, and total octahedral R^{2+} cations at the apices. Celadonite points are open circles; glauconites, closed circles. Substitution of the type MgSi. AlAl takes place parallel to the line joining tetrasilicic celadonite and muscovite. Data sources are the same as for Fig. 2.

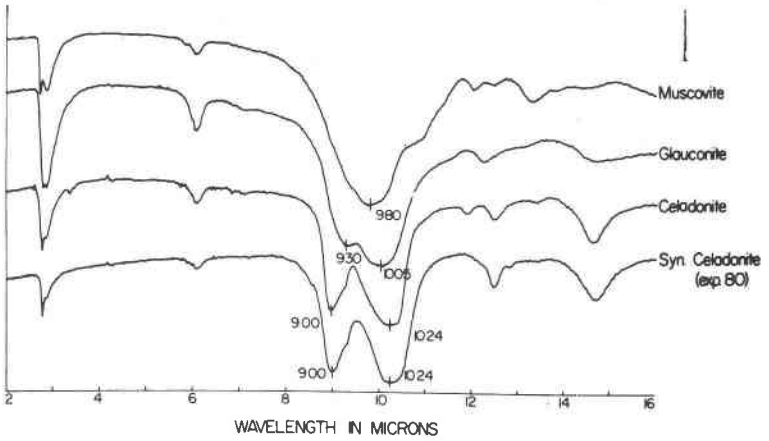

FIG. 5. Infra-red absorption spectra for a muscovite (from a pegmatite, San Diego County, Cal.), glauconite (from Santa Monica Bay, provided by W. L. Pratt), celadonite and a synthetic celadonite (exp. 80). In addition to the Si-O absorption bands between 8 μ and 11 μ, the O-H band is at 2.81 μ. The absorption at 2.90 μ is probably absorbed water in the specimen and KBr disk.

an additional group of end members, those of the series muscovite-ferrimuscovite:

$KAl_2AlSi_3O_{10}(OH)_2$ (5) and
$KFe_2^{3+}AlSi_3O_{10}(OH)_2$ (6) (see Fig. 17)

Although there were separate fields for celadonite and glauconite (Fig. 4) with some overlap, chemical analyses are necessary in order to distinguish them on this basis. For example, two of the "secondary glauconites" from an iron-formation in Minnesota (Tyler and Bailey, 1961) plot within the celadonite field and the third is near the glauconite field, but not out of that for celadonite. These three micas, then, probably should be considered celadonites.

Infrared absorption spectra. Tuddenham and Lyon (1959), Lyon and Tuddenham (1960), Lyon (1963) and Liese (1963) have shown that the amount of tetrahedral aluminum in phyllosilicates can be qualitatively determined from infrared absorption analysis. The spectra of dioctahedral micas with less than 0.20 tetrahedral aluminum (Fig. 1) are clearly different from those micas with more tetrahedral aluminum. Lyon and Tuddenham (1960) and Lyon (1963) illustrate these differences but did not apply them to the problem of glauconite and celadonite terminology.

Between the wavelengths of 8 μ and 12 μ glauconite and celadonite have different absorption spectra (Fig. 5), showing that they may have some

compositional and/or structural differences. Celadonite has absorption peaks at 9.00 μ and 10.24 μ, whereas glauconite has either one peak near 9.80 μ (Lyon, 1963), two peaks at 9.30 μ and 10.05 μ (Fig. 5) or two at 9.4 μ and 10.2 μ (Owens and Minard 1960). The single peak at 9.80 μ of glauconites is in the same position as that in the spectra of muscovites. Absorption peaks in dioctahedral layered silicates between 9 μ and 11 μ are attributed to Si-O bond stretching (Lyon, 1963, p. 29, and Farmer, 1958, p. 834). Muscovite with greater than 0.30 tetrahedral aluminum has one peak at 9.80 μ. However, two peaks occur in this region when the amount of tetrahedral aluminum approaches zero, such as for chlorites, lepidolites, and dioctahedral micas studies by Lyon and Tuddenham.

The spectra of celadonites (less than 0.30 tetrahedral aluminum) are consistent with those of the other layered silicates with low tetrahedral aluminum. The glauconite spectra, which appear to be often the same as those of muscovite, show that the amount of tetrahedral aluminum is nearer that of muscovite and is distinctly different from that of celadonite. Both celadonite and muscovite can be identified in artificially prepared mixtures. It should be possible to recognize natural mixtures of celadonite and illite using this technique, although not possible for glauconite and illite.

Just as the two fields for glauconite and celadonite overlap in Fig. 4, the absorption spectra for these samples probably would show an overlap. However, it seems unwise to alter the usage of the terms celadonite and glauconite from the traditional, where the names refer to occurrence rather than strictly composition. The infrared absorption spectra provide a means for the distinction without chemical analysis.

The glauconite problem. Radoslovich (1963b, p. 357), in considering the stable structures of the muscovites, illites and celadonites, was concerned mainly with the effects of substitution of aluminum into the octahedral layer. He assumed the existence of a structural discontinuity between muscovite and celadonite and indicated the limits of the two structure types. He says that there is a "lower limit for Al^{VI} required for the stable muscovite structure" and concludes that glauconites cannot have the muscovite structure and, therefore, must be represented by mixed structures. Data presented earlier suggests that the latter part of this statement may not be true.

The chemical data in Fig. 3 indicate that the chemical composition, as expressed by Fe^{3+}/Al and Mg/Fe^{2+} ratios, of the octahedral layers of celadonites and glauconites is in general the same. The analysis of a mixture of celadonite and illite should have a lower Fe^{3+}/Al ratio than celadonites alone. The chemical differences between celadonites and glauco-

nite arise from the substitution of aluminum into the tetrahedral layer, which must be accompanied by the substitution of a trivalent cation for a divalent one in the octahedral layer, which will not be reflected in the Fe^{3+}/Al ratio. These substitutions are of the type $MgSi \rightleftharpoons 2Al$, or more specifically expressed by

$$(Mg, Fe^{2+})^{VI}S^{IV} \rightleftharpoons (Fe^{3+}, Al)^{VI}\,Al^{IV}.$$

Infrared absorption spectra indicate that all the purified glauconites, analyzed so far using this method, probably are not mixtures of the two minerals. Therefore, the writers prefer the view that glauconites have the same structure as celadonite, but contain more tetrahedral aluminum and more octahedral R^{3+} cations.

X-ray and optical properties. *X*-ray powder patterns of natural celadonites are similar to those of the natural 1M muscovites illustrated by Yoder and Eugster (1955). An indexed powder pattern of the celadonite No. 15 is shown in Fig. 5. Powder data and cell dimensions are given in Tables 3 and 4, respectively. *X*-ray powder data given by Schüller and Wohlmann (1951) and Bayramgil, *et al.* (1952) are similar with small variations. The peak with a spacing of about 3.32 Å is the third order basal peak, 003 (or 006 for 2M polymorphs). The two peaks with spacing of 3.64 Å and 3.09 Å, can only be indexed on a 1M cell and are $11\bar{2}$ and 112, respectively.[1] These peaks are present in all published *x*-ray powder patterns of celadonite and in those of other celadonites studied by the writers. Therefore, all of these natural celadonites are the 1M polymorph. Peaks characteristic for 2M polymorphs ($11\bar{4}$ and 114 with spacings of 3.50 Å and 3.12 Å) have never been observed.

Published *x*-ray powder data for celadonites is far too meager to allow any variations in $d_{(060)}$ or $d_{(003)}$ to be used for composition determinations. Data available is given in Tables 1 and 3. Variations in $d_{(060)}$ have been related to the $Mg:Fe^{2+}$ ratios in biotites (Wones, 1958), but a similar relationship for natural celadonites is not apparent from Table 1. The amount of tetrahedral aluminum may also be important, since muscovite has a $d_{(060)}$ of 1.500 Å.

Refractive indices of natural celadonites range between 1.64 and 1.58. Hutton and Seelye (1941) were able to show that the refractive indices of glauconites increase with increasing Fe^{3+} content. A similar relationship appears to be true here, especially for celadonites, 1, 3, 15, 16 and 19 in

[1] It should be noted here that the β angle defined by the $11\bar{2}$ and 112 reflections for celadonites departs from that for 1M muscovite (Table 4) toward the β angle characteristic of trioctahedral micas, possibly accounted for by an extra thick octahedral layer (Radoslovich, 1963a, p. 94).

TABLE 3. *X*-RAY POWDER DATA FOR CELADONITE FROM THE WIND RIVER AREA, WASH. CuK$_\alpha$ RADIATION, NI FILTER

hkl	$d_{calc.}$	$d_{obs.}$	I
001	9.94	9.97	47
020	4.53	4.53	85
11$\bar{1}$	4.36	4.35	42
021	4.123	4.14	37
11$\bar{2}$	3.638	3.635	80
022	3.349	3.35[1]	60
003	3.314	3.318[1]	70
112	3.081	3.087	80
11$\bar{3}$	2.901	2.90 B	10
023	2.675	2.678	75
130	2.605	2.604	70
13$\bar{1}$	2.581	2.580	100
13$\bar{2}$	2.404	2.402	75
040	2.265	2.264	18
041	2.208	2.209	25
13$\bar{3}$	2.150	2.148	31
202	2.125		
005	1.988	2.092	10
151	1.665	1.65 B	15
060	1.510	1.509	60

[1] The exact location of these two peaks is difficult to obtain.

B broad peak.

Observed data from diffractometer traces with silicon (a=5.4306 Å) as an internal standard.

TABLE 4. CELL DIMENSIONS OF NATURAL CELADONITE (WIND RIVER AREA, WASH.)

a= 5.23 (±.02) Å
b= 9.06 (±.01) Å
c=10.13 (±.02) Å
β=100° 55′ (±10′)

Cell dimensions of 1M Muscovite (Yoder and Eugster, 1955)

a= 5.208
b= 8.995
c=10.275
β=101° 35′

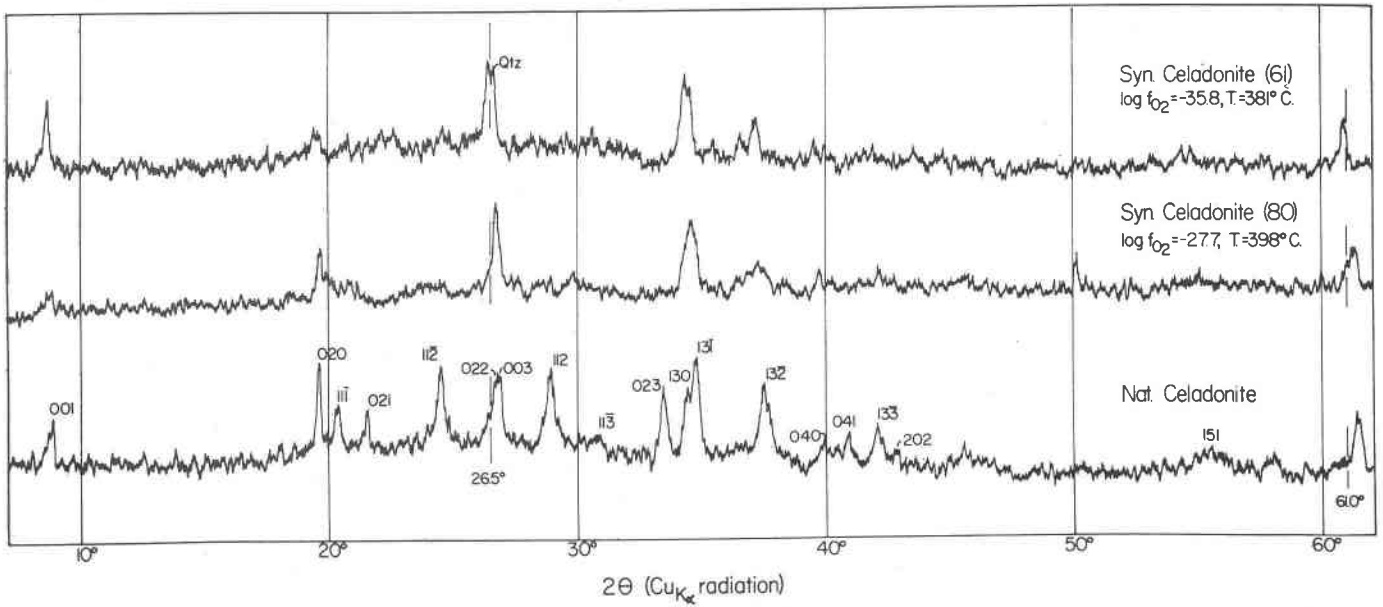

FIG. 6. *X*-ray diffractometer patterns for natural celadonite and two synthetic $MgFe^{3+}$-celadonites, grown at different oxygen fugacities. For d-spacings of these patterns see Tables 3 and 6.

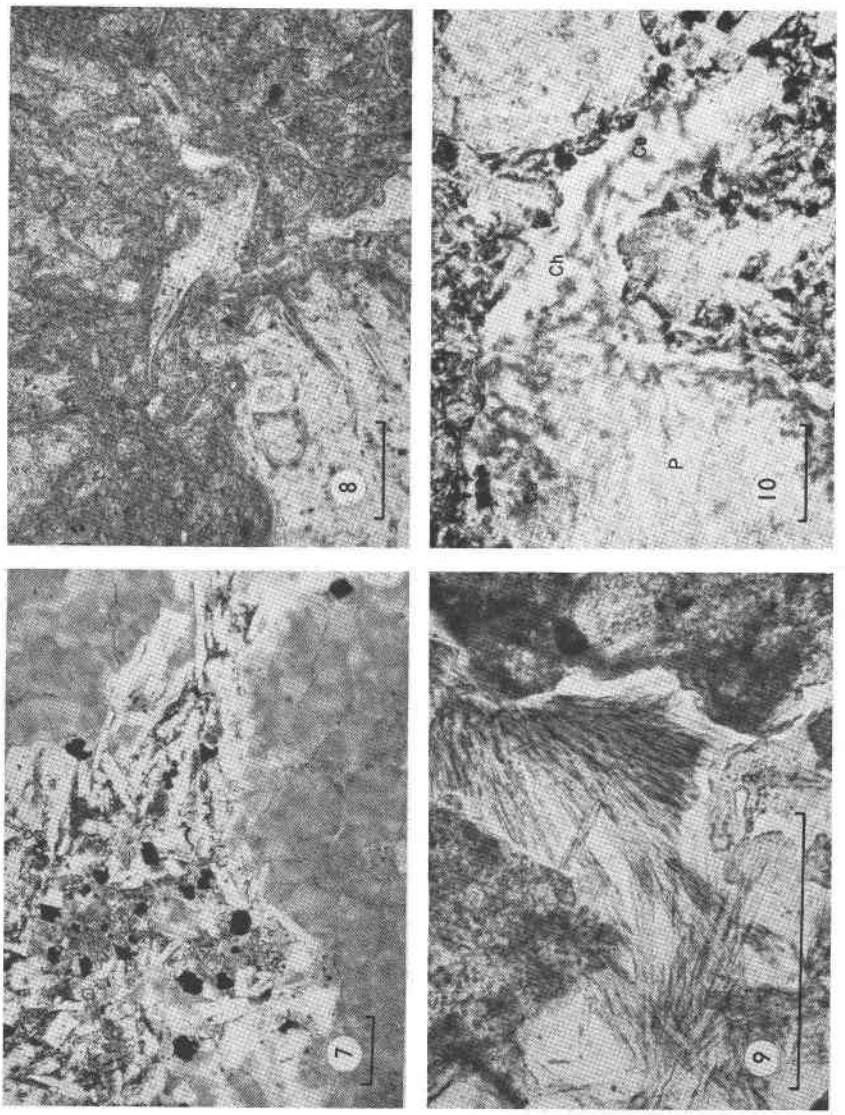

FIG. 7. Photomicrograph of celadonite amygdule fillings in a basalt from Washington. Plane polarized light. 90×. Length of bar is 0.1 mm.

FIG. 8. Photomicrograph of zeolitized tuff of John Day formation of Oregon. Light areas are clinoptilolite; most of the darker area is a fine intergrowth of montmorillonite and celadonite with clinoptilolite. Plane polarized light. 130×. Length of bar is 0.1 mm.

FIG. 9. Photomicrograph of balded celadonite growing with heulandite in a pore space of a volcanic sandstone. The dark area on the right side and upper left corner are zeolitized

Table 1. However, the data are so few and other possible variables so numerous that definite composition determinations using refractive indices are not yet possible.

Occurrences of celadonite. The blue-green color of certain altered tuffaceous rocks has long been attributed to the presence of celadonite, although positive identification was lacking until *x*-ray diffraction methods were employed. Prior to about 1950 celadonite occurrences recorded in the literature were chiefly those of cavity fillings in basalts and andesites. The following is a summary of known celadonite occurrences and of mineral assemblages of which celadonite is a member.

a. Occurrences in amygdules and fractures of altered lavas

Most of the analyzed celadonites given in Table 1 come from amygdule or fracture fillings in basalt or andesites, which are largely Mesozoic to middle Tertiary in age. These basic lavas are moderately to highly altered, *i.e.* at least devitrification of the glass has taken place. Celadonite fills vesicles, usually in the lower parts of the flows. In the more highly altered basalts and especially in the vesicular portions of the flows, celadonite also replaces plagioclase and pyroxene grains (Fig. 7). Ross and Hendricks (1941, p. 685) report the replacement of olivine and hypersthene phenocrysts as well as groundmass material.

The minerals most commonly associated with celadonite in these occurrences are montmorillonite and chalcedony or quartz. Montmorillonite is usually easy to distinguish from celadonite in thin section because of the yellow-brown pleochroic colors in contrast to the yellowish-green to blue-green of celadonite. Small amounts of included chalcedony and quartz cannot be seen in thin sections, because the intergrowths are very fine grained. The small silica content must be identified by *x*-ray methods. Larger quantities of quartz or chalcedony cause the amygdule or fracture fillings to have a hardness greatly exceeding that of the pure, earthy celadonite (H = 1 to 2).

b. Altered volcanic clastic rocks

Volcanic clastic rocks upon diagenetic alteration or low grade metamorphism (zeolite facies) often develop celadonite bearing assemblages.

---

lava sand grains. Celadonite blades show the differences in absorption. Plane polarized light. 365×. Length of bar is 0.1 mm.

FIG. 10. Photomicrograph of prehnite-chlorite-celadonite amygdule fillings in a metavolcanic rock from the Sparta Quad., Oregon. Ch—chlorite, Ce—celadonite and P—prehnite. Plane polarized light. 130×. Length of bar is 0.1 mm.

Celadonite in altered volcanic clastic rocks has been found in New Zealand (Coombs, 1954; Coombs *et al.*, 1959), Japan (Sudo, 1951, 1953), and has been long recognized in the Pacific northwest of the United States and recently reported by Fiske (1960); Wise (1961); and Hay (1961, 1963). It is interesting to note that in most of these occurrences the celadonite is associated with zeolite or another calcium-aluminum silicate, such as prehnite. For convenience the following descriptions are divided into four groups, which are roughly comparable to the stages of the zeolite facies of Coombs *et al.* (1959) and the prehnite-pumpellyite facies (Coombs, 1961).

(i). Clinoptilolite-bearing assemblages

Excellent examples of celadonite bearing assemblages of this association occur in the John Day formation of central Oregon. Volcanic glass and, to a far lesser extent, pyroxenes have been altered to assemblages containing clinoptilolite, celadonite, and montmorillonite (Hay, 1961; Fisher, 1963). From specimens made available to the writers by R. V. Fisher, the following assemblages were observed:

celadonite-montmorillonite-quartz-clinoptilolite
celadonite-quartz-clinoptilolite
celadonite-montmorillonite-clinoptilolite
celadonite-clinoptilolite (and heulandite)

The celadonite in the tuffs of the John Day formation has replaced pumice fragments and some of the larger glass shards. The complete crystallization or replacement of a glass shard by zeolite occasionally produces celadonite (Fig. 8). Hay (1963) regards many of these larger areas as fillings of cavities which were formed by complete solution of the original shard. The fillings of bubbles in pumice fragments exhibit similar structures.

Celadonite replacing the fine glass fragments and pumice is very fine grained but easily identified by the color coupled with the high birefringence. In the cavity fillings the plates of celadonite are large enough to exhibit the characteristic pleochroism.

(ii). Heulandite-bearing assemblages.

Celadonite, occurring in rocks of a slightly higher grade of metamorphism has been reported in the following assemblages:

analcite-celadonite-quartz
heulandite-celadonite-quartz (-sphene)
(Coombs *et al.* 1959)

From the Wind River area, Washington, the following assemblages were observed by Wise (1961):

celadonite-heulandite-quartz-montmorillonite
celadonite-heulandite-quartz
celadonite-heulandite-chlorite
celadonite-heulandite-quartz-montmorillonite-calcite
heulandite-quartz-celadonite-chlorite: montmorillonite (mixed layer)
celadonite-heulandite-analcite-quartz-chlorite

These assemblages are most easily recognized and identified where the minerals have replaced the glassy portions of the volcanic clastic rocks. Intergrain spaces in all of the epiclastic rocks are filled with a zeolite and one or more of the above layered silicates (Fig. 9). Quartz is very fine grained in these rocks and can only be identified through *x*-ray methods.

(iii). Laumontite-bearing assemblages.

Coombs *et al.* (1959, p. 60) report the following assemblages:

celadonite-laumontite-albite-quartz-sphene
celadonite-laumontite-albite-adularia-quartz

Also in associated rocks:

albite-quartz-chlorite-sphene
albite-chlorite-calcite-sphene

It is interesting to note that the laumontite rocks from the Wind River area, Washington, contained only chlorite as the layered silicate mineral. Dickinson (1962) reports that celadonite has apparently altered to chlorite in the Triassic laumontite rocks from the Izee area, Oregon. Ross (1958) reports celadonite with chlorite, saponite, and laumontite replacing welded tuffs in deep wells in Georgia but does not indicate possible equilibrium assemblages.

(v). Prehnite-bearing assemblages

Coombs, *et al.* (1959) and Coombs (1960) do not indicate that celadonite occurs in any of the prehnite-pumpellyite metagraywackes or metavolcanics of New Zealand. However, samples of metavolcanics (spilitic?) from the Sparta quadrangle, eastern Oregon (courtesy of H. Prostka) have the assemblages—celadonite-chlorite-prehnite (see Fig. 10) and celadonite-prehnite-pumpellyite (Prostka, personal communication). Also some volcanic clastic rocks from Mt. Rainier National Park (courtesy R. S. Fiske) have the assemblage—celadonite-prehnite. In both of these examples the celadonite can be recognized in the thin section by its birefringence and blue-green color; seldom is it coarse grained enough to see the pleochroism.

c. Glauconite

The mineral heterogeneity of glauconite pellets has been carefully described by Burst (1958) and others. The origin of the glauconite in these

pellets is not clear, and glauconite is regarded by many as a replacement mineral. It is difficult to determine whether the glauconite in these pellets is in equilibrium with the associated montmorillonite, chlorite, or quartz. Since both celadonite and glauconite and illite have nearly the same basal spacings, the common methods of identification (see Burst, 1958, p. 484) make it nearly impossible to distinguish glauconite and illite in the same sample. If both phases are present, the (060) peak for each should be present. Infrared spectra of glauconites and illites are nearly identical (Fig. 5) and are, therefore, of no use.

Experimental Results

Experimental techniques. Experiments, making use of the usual hydrothermal techniques, were undertaken to synthesize the celadonite end members and to determine the stability relations of celadonite. Since the bulk composition contains iron, the fugacity of oxygen (f_{O_2}) plays an important role in addition to P_{H_2O} and temperature in controlling the stability and composition of celadonite and the high temperature phases. Therefore, the oxygen buffer techniques of Eugster (1957) were used. For a detailed discussion of these see Eugster and Wones (1962).

The fugacity of oxygen was controlled by the following buffers:

hematite+magnetic	(HM)
nickel+nickel oxide	(NNO)
quartz+fayalite+magnetite	(QFM)
iron+magnetite	(IM)

The f_{O_2}-T curves for these buffers, corrected for the effect of 2,000 bars, were calculated from data given by Eugster and Wones (1962) and are plotted in Fig. 12. Recent direct calibrations of the NNO and QFM buffers at 700° C. (Shaw, 1963) show surprisingly good agreement with the calculated values. Equipment for pressure and temperature control and measurement was essentially that described by Eugster and Wones (1962). Silver capsules were used inside the platinum tubes to prevent loss of iron into the platinum.

Many of the starting materials used were glasses or synthetic minerals, grown from glasses. These glasses were prepared by heating mixtures of $KHCO_3$ and quartz with MgO, Fe_2O_3, or γ-Al_2O_3, depending on the composition desired. The heating was carried through the same series of steps outlined by Schairer and Bowen (1955) for the preparation of potassium-silica glasses. For some of the experiments a reduced glass was used; this glass was prepared by placing a glass, made in the above manner, in a stream of hydrogen for two or three hours at 700° C. Mixes used in some of the experiments were prepared from K_2O-SiO_2 glasses (Schairer and Bowen, 1955), mixed with MgO and γ-Al_2O_3. MgO was made by heating

$MgCO_3$ at 900° C. for an hour, and the γ-Al_2O_3, by heating $AlCl_3 \cdot 6H_2O$ at 700° and 900° C. for a few hours. No mixes were used for critical runs establishing phase boundaries.

Description of synthetic phases. The $MgFe^{3+}$-celadonite grows readily from a glass of the appropriate composition between 300° and 430° C. with all oxygen buffers used. For examples of specific synthesis conditions see Table 5. Individual grains are too small to be recognized under the microscope. Consequently only a mean refractive index can be measured. The color of synthetic celadonite is variable within the range blue-green

TABLE 5. PROPERTIES OF SYNTHETIC $MgFe^{3+}$-CELADONITES

Exp. No.	Buffer	log f_{O_2} bars	Temp. °C	Pressure bars	N_m	$d_{(060)}$ Å	$d_{(003)}$ Å
37	HM	−20.5	430	2,000	1.621	1.512	3.320
71	NNO	−26.5	418	1,000	1.620	1.514	3.335
81	NNO	−27.0	414	1,000	1.620	1.514	3.351
59	NNO	−27.0	414	2,000	1.620	1.515	3.34
80	NNO	−27.7	398	2,000	—	1.516	3.352
60	QFM	−28.5	412	2,000	1.621	1.513	3.34
83	QFM	−29.0	418	1,000	1.620	1.514	—
51	QFM	−31.0	398	2,000	—	1.515	3.35(?)
61	IM	−35.8	381	2,000	—	1.521	3.368
62	IM	−36.3	377	2,000	1.618	1.517	—
56	IM	−37.2	360	2,000	—	1.521	3.37
41	IM	−37.5	355	2,000	1.618	1.519	3.372

to apple-green. The variation seems to depend more on the duration of the run than on the fugacity of oxygen or temperature.

Celadonites synthesized with the (HM) and (NNO) buffers (Table 8) contain less than 3 per cent additional phases. The only phase to be detected by optical or x-ray methods is quartz, and the amount of quartz increases as the fucagity of oxygen decreases. Figure 6 shows the x-ray patterns of two synthetic celadonites, one of which also shows a quartz peak. This latter celadonite (exp. 61) contains less than 10 per cent quartz.

The properties of the synthetic $MgFe^{3+}$-celadonite are strongly controlled by the fugacity of oxygen. The b and c cell dimensions show a steady increase with increasing f_{H_2} (or decreasing f_{O_2}). These changes measured by $d_{(060)}$ and $d_{(003)}$ are tabulated in Table 5 and illustrated in Fig. 11 a and b. The (060) peaks are usually broad and weak and measurements are probably accurate only to $\pm 0.03°$ 2θ (± 0.001 Å). Most

patterns were measured using an external standard. However, when sufficient material was available oscillation patterns with a silicon internal standard were used.

The lowest $d_{(060)}$, 1.512 Å, and the lowest $d_{(003)}$, 3.320 Å, were obtained from the celadonite grown at the highest f_{O_2} (HM buffer, exp. 37). The

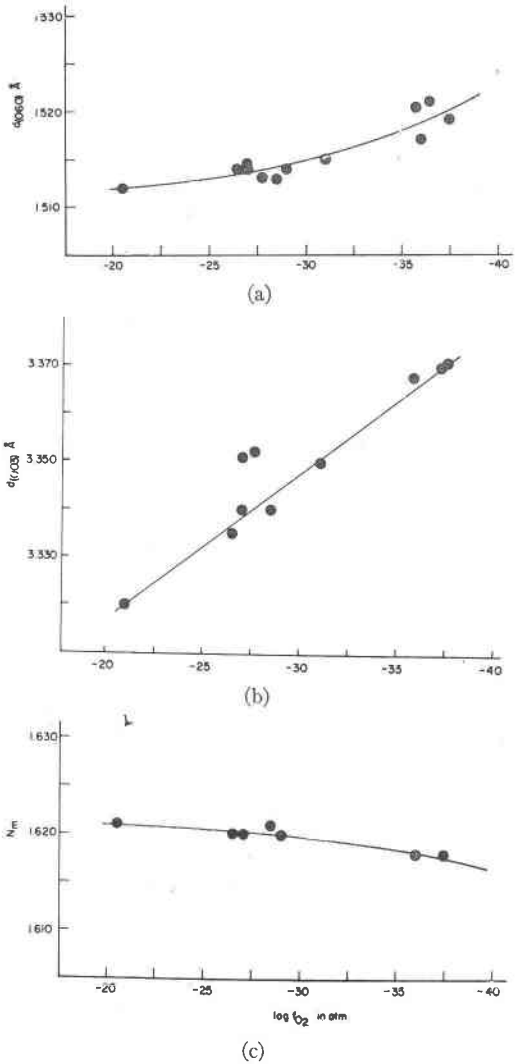

FIG. 11. Properties of synthetic celadonites (Table 5).

a. Plot showing variations of $d_{(060)}$ with f_{O_2}.
b. Plot showing the variation of $d_{(003)}$ with f_{O_2}.
c. Plot showing the variation of refractive index with f_{O_2}.

highest $d_{(060)}$, 1.521 Å, and highest $d_{(003)}$, 3.372 Å, were measured on the celadonite, grown from the high temperature phases with an IM buffer for two weeks at 360° C. (exp. 56). With increasing $d_{(060)}$ there is a corresponding increase of $d_{(003)}$ with increasing f_{H_2} (or decreasing f_{O_2}, see Table 5 and Figs. 11a and 11b).

The mean refractive index (measured by oil immersion methods in white light with oils calibrated in Na light) of the synthetic celadonites varies only slightly with increasing f_{O_2}, but the change is constant and measurable (Table 5, Fig. 11c).

Similar changes in optical properties and cell dimensions of hydrous iron silicates have been noted by Ernst (1960) (magnesioriebeckite), Ernst (1962) (riebeckite), and by Eugster and Wones (1962) (annite). Ernst interprets the change to arise from the reduction of the ferric iron of the magnesioriebeckite, as the f_{H_2} increases. Eugster and Wones say that with increasing f_{O_2} the ferrous iron in annite is oxidized, coupled with a removal of hydrogen (solid solution with "oxyannites").

The observed changes in the N_m, $d_{(003)}$, and $d_{(060)}$ of the synthetic celadonites might be accounted for in one or more of the followings ways:

1. With high f_{H_2} some of the ferric iron is reduced and hydrogen is added. Such a celadonite might have the formula:

$$KMgFe_x^{+2}Fe_{1-x}^{+3}Si_4O_{10-x}(OH)_{2+x}$$

This is similar to a process proposed by Zussman (1955) for actinolites.

2. Reduction of ferric iron could also be accomplished by solid solution (or mixed layering) with the $Fe^{2+}Fe^{3+}$-celadonite or even ferriannite, $KFe_3^{2+}Fe^{3+}Si_3O_{10}(OH)_2$. In either case there would have to exist phases containing excess potash, magnesia, and silica. No such phases have been observed with the exception of quartz.

3. At high f_{O_2} some of the hydrogen may be lost leading to "oxyceladonite." Coupled with such a reaction, there must be an excess of ferric iron in the octahedral positions. According to the formula:

$$KMgFe_{1+x}^{3+}Si_4O_{10+x}(OH)_{2-x}$$

Again, phases should have formed to accommodate the excess potash, magnesia and silica.

Of these three possibilities the first seems the most likely, judging from the lack of other phases accompanying the celadonite. The reduction in amount of ferric iron is consistent with the decrease in N_m. The increase of ferrous iron in the octahedral positions may produce the high values for $d_{(060)}$ (the ionic radius of Fe^{2+} is 0.74 Å as compared with 0.64 Å for Fe^{3+}). Interlayering or solid solution with ferriannite or $Fe^{2+}Fe^{3+}$-celadonite would also produce an increase in $d_{(060)}$.

The synthetic celadonites from very short runs are of the disordered, 1Md, type (Yoder and Eugster, 1955), since only basal peaks appear. Celadonites grown at the highest temperatures show only 1M peaks. Only a small number of the expected (hkl) reflections are present (Fig. 6,

Table 6), and the patterns are too poor to calculate accurate cell dimensions.

Ferribiotite, $KMg_{3-x}Fe_x^{2+}Fe^{3+}Si_3O_{10}(OH)_2$ with $1>x>0$, is present in all of the high temperature synthetic assemblages. In the high f_{O_2} regions the ferribiotite is nearly pure ferriphlogopite, $KMg_3Fe^{3+}Si_3O_{10}(OH)_2$. But at low f_{O_2} values ferrisanidine melted incongruently to ferriannite and liquid:

$$4KFe^{3+}Si_3O_8 \rightleftarrows KFe_3^{2+}Fe^{3+}Si_3O_{10}(OH)_2 + \text{liquid}.$$

Since ferriphlogopite and ferrisanidine are present in the celadonite bulk

TABLE 6. *X*-RAY POWDER DATA FOR SYNTHETIC $MgFe^{3+}$-CELADONITE (THE TRACES FOR FOLLOWING TWO CELADONITES ARE SHOWN IN FIG. 5)

Silicon was used as the internal standard ($a=5.4306$ Å).

Syn. Celadonite (#61) log $f_{O_2}=-35.8$ atm. Temp.$=381°$ C.			Syn. Celadonite (#80) log $f_{O_2}=27.7$ atm. Temp.$=398°$ C.	
hkl	I	d Å	I	d Å
001	70	10.2	22	10.50
020	30	4.53	33	4.53
—	20	4.27	—	—
003	100	3.368	100	3.352
$13\bar{1}$?	73	2.608	55	2.595
—	—	—	13	2.46
$13\bar{2}$?	40	2.49	20	2.42
040	—	—	9	2.26
060	30	1.521	27	1.516

composition in a proportion of 1:2, the ferribiotite must be a member of the ferriphlogopite-ferriannite solid solutions with a 2:1 ratio (hence, x in the ferribiotite formula given above is nearly equal to 1).

At low temperatures, *i.e.* below 450° C., the ferribiotite is exceedingly fine-grained, and individual crystals cannot be detected. However, above 500° C. the grains grow to near 10 microns in diameter. All ferribiotites are brown and pleochroic. Pure ferriphlogopite has the following optical properties:

$\alpha = 1.600 \pm .001$ (measured in white light with
$\beta \simeq \gamma = 1.642 \pm .001$ oils calibrated in Na light)
$\gamma - \alpha = 0.042$
$2V_x = 0$ or very small
pleochroic scheme X = reddish-brown
Y = Z = colorless
X > Y = Z

TABLE 7. *X*-RAY POWDER DATA FOR SYNTHETIC FERRIPHLOGOPITE, COMPARED TO THAT FOR SYNTHETIC FERRIANNITE (WONES 1963), AND SYNTHETIC PHLOGOPITE (YODER AND EUGSTER, 1954)

None of these lists of d-spacings represent all of the reflections.

hkl	ferriannite	ferriphlogopite		phlogopite
	d	d	I	d
001	10.18	10.14	72	10.16
002	5.08	5.09	27	5.08
020	—	4.63	22	4.60
110	4.66	4.59	20	4.55
111	—	3.96	10	4.12
11$\bar{2}$	3.736	3.695	38	3.672
022	3.456	3.430	62	3.409
003	3.394	3.142	100	3.387
112	—	3.182	68	3.163
11$\bar{3}$	2.95	2.950	35	2.944
023	—	2.743	20	2.728
130 20$\bar{1}$	—	2.667	32	2.646
200 13$\bar{1}$	2.673	2.633	98	2.169
004	2.545	2.550	25	2.541
		2.530	18	
13$\bar{2}$ 201	—	2.454	43	2.435
220	—	2.285	10	2.272
041	—	2.234	5	2.244
22$\bar{2}$	—	2.219	7	2.204
13$\bar{3}$ 202	2.212	2.194	32	2.179
005 113	2.031	2.041	38	2.032
20$\bar{4}$ 133	—	2.006	22	2.002
20$\bar{5}$ 134	—	1.765	10	1.757
13$\bar{5}$ 204	1.699	1.692	35	1.684
		1.657	10	1.645
060	1.567	1.547	62	1.534

Ferriphlogopite data were measured from a diffractometer pattern with silicon (a=5.4306 Å) as an internal standard.

The x-ray powder pattern for ferriphlogopite is given in Table 7, together with those for synthetic ferriannite and synthetic phlogopite. The unit cell dimensions of the ferriphlogopite, calculated from the powder data of Table 7, are:

$$a = 5.34\ \text{Å}(\pm .01)$$
$$b = 9.28\ \text{Å}(\pm .005)$$
$$c = 10.35\ \text{Å}(\pm .01)$$
$$\beta = 99°55'\ (\pm 10')$$

Steinfink (1962) gave the following cell data for a naturally occurring ferriphlogopite:

a = 5.36 Å; b = 9.29 Å; c = 10.41 Å; β = 100° 00′

The cell dimensions of the other synthetic biotite end members: phlogopite (Yoder and Eugster, 1954):

$a = 5.314$ Å; $b = 9.204$ Å; $c = 10.314$ Å; $\beta = 99° 54'$

annite (Eugster and Wones, 1962):

$a = 5.39$ Å; $b = 9.334$ Å; $c = 10.290$ Å; $\beta = 100° 00'$

ferriannite (Wones, 1963):

$a = 5.430$ Å; $b = 9.404$ Å; $c = 10.341$ Å; $\beta = 100° 04'$

Ferribiotite containing some ferrous iron has a powder pattern similar to that of pure ferriphlogopite. However, the $d_{(060)}$ reflection has shifted toward the 1.567 Å value of ferriannite. This peak is difficult to measure because of the interference from coexisting quartz. However, a similar shift was observed when pure ferriphlogopite was equilibrated at an f_{O_2} of $10^{-29.5}$ atm at 490° for one week. This shift probably was due to the reduction of ferric iron in a process similar to that for celadonite discussed earlier. Therefore, $d_{(060)}$ cannot be used to determine the $Mg:Fe^{2+}$ ratio of ferribiotite.

Ferrisanidine in all of the runs was intimately mixed with ferribiotite and quartz, so that its optical properties could not be determined with any precision. The γ-index is near 1.600, which is in accord with the data of Wones and Appleman (1961), who give the following values.

$\alpha = 1.584$
$\beta = 1.595$
$\gamma = 1.605$

Ferrisanidine was identified on the x-ray powder patterns of the runs by the presence of the following peaks:

(130)	3.81 Å
$(\bar{2}20)$ $(\bar{2}01)$	3.35 Å
(040) (002)	3.27 Å
(131)	3.02 Å

(Indices are from Wones and Appleman, 1961.)

In view of a recent paper by Wones and Appleman (1963) it is somewhat disturbing to note that the iron feldspar encountered in this study is ferrisanidine rather than ferrimicrocline. The four peaks, given above, were found on x-ray patterns from all runs yielding the high temperature assemblages. We can only suggest that the runs were of such a short duration and low temperature that the iron microcline did not have time to grow.

In runs above the stability limit of celadonite on the (QFM) and (IM)

buffers, a glass was found (Fig. 12). The glass is colorless and has a refractive index between 1.510 and 1.514. (The intimate intergrowth of the glass with ferribiotite flakes makes a more accurate determination impossible.) The glass was found to be present in runs at temperatures as low as 405° C. and 2,000 bars P_{H_2O}. Roedder (1952) found a glass on the

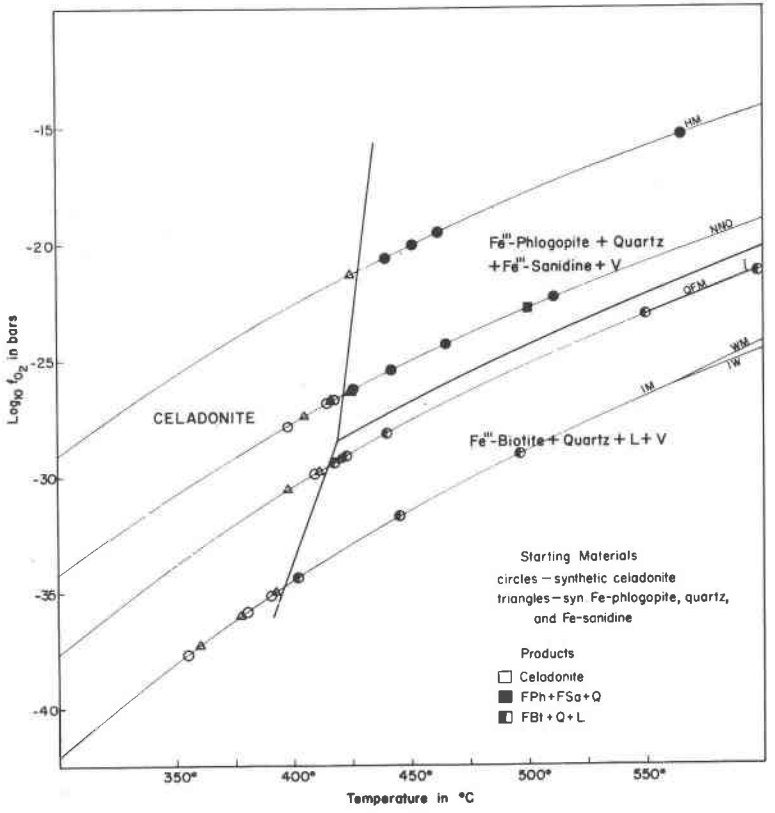

FIG. 12. f_{O_2}-T diagram at 2,000 bars total pressure for the bulk composition $K_2O \cdot 2MgO \cdot Fe_2O_3 \cdot 8SiO_2$ with excess water. See Table 8 for the abbreviations used.

$K_2O \cdot 4SiO_2$-FeO join, with about 10% FeO and 1% Fe_2O_3 to have a refractive index of 1.52. This glass crystallizes at 1 atm at a temperature which may be as low as 700° C.

Thermal stability of the $MgFe^{3+}$-celadonite. The stability of the $MgFe^{3+}$-celadonite was investigated at a constant total pressure ($P_{total} = P_{H_2O} + P_{H_2}$) of 2,000 bars with temperature and oxygen fugacity as variables. For f_{H_2} values of the oxygen buffers used see Eugster and Wones (1962).

Only a few experiments were performed at 1,000 bars, and most of these on the (NNO) buffer. Experimental data are listed in Table 8 and plotted on Fig. 12.

The three starting materials for these experiments are synthetic celadonite (Cel), and the synthetic high-temperature assemblages quartz ferriphlogopite+ferrisanidine (QPS) and ferrisanidine+quartz+liquid

TABLE 8. RUN DATA FOR THE EXPERIMENTS WITH OXYGEN BUFFER CONTROL ON CELADONITE, $KMgFe^{3+}Si_4O_{10}(OH)_2$
(selected runs only)

Abbreviations used: Cel —celadonite
FPh—ferriphlogopite
FBt —ferribiotite
FSa —ferrisanidine
QPS—quartz+ferriphogopite+ferrisanidine
SQL—ferrisanidine+quartz+liquid
L —liquid
Q —quartz
brackets around phases which are thought to be metastable

Exp. No.	Starting Material	Temp. (°C)	Time (hrs.)	Condensed Phases
		$P_{vapor}=2,000$ bars		
		Hematite-magnetite buffer		
72	QPS	424	165	Cel+[FPh+FSa+Q]
37	Cel	430±6	240	Cel
75	Cel	439	270	[Cel]+FPh+FSa+Q
68	Cel	453	190	FPh+FSa+Q+[Cel]
54	Cel	475	290	FPh+FSa+Q
34	Cel	570	120	FPh+FSa+Q
		Nickel-nickel oxide buffer		
80	Cel	398	960	Cel
50	QPS	405	240	Cel+[FPh+FSa+Q]
59	Cel	414	335	Cel
67	QPS	416	335	FPh+FSa+Q
32	Cel	417	160	Cel
42	QPS	424	332	FPh+FSa+Q
53	Cel	426	335	FPh+(FSa)+Q+[Cel]
39	Cel	442	155	FPh+FSa+Q+[Cel]
26	Cel	465	165	FPh+FSa+Q
106	SQL	498	90	FPh+FSa+Q
24	Cel	511	265	FPh+FSa+Q
31	Cel	749	120	FPh+L

TABLE 8—(*Continued*)

Exp. No.	Starting Material	Temp. (°C)	Time (hrs.)	Condensed Phases
		Quartz-fayalite-magnetite buffer		
51	QPS	398	240	Cel+[FBt+Q]
60	Cel	412	500	Cel
63	QPS	412	335	Cel+[FBt+Q]
66	Cel	418	165	FBt+Q+L?+[Cel]
49	QPS	420	335	FBt+Q+L+[FSa]
36	Cel	423	240	FBt+Q+L+[Cel]
55	Cel	440	290	FBt+Q+L+[Cel]
97	QPS	550	120	FBt+Q+L
35	Cel	599	120	FBt+Q+L
		Iron-magnetite buffer		
41	Cel	355	330	Cel+Q
56	QPS	360	335	Cel+[FBt+Q]
62	QPS	377	165	Cel+[FBt+Q]
61	Cel	381	455	Cel+Q
64	Cel	391	165	Cel+Q
65	QPS	392	192	Cel+[FPh+FSa+Q]
33	Cel	402	180	FBt+Q+L
40	Cel	450	168	FBt+Q+L
98	Cel	495	165	FBt+Q+L
		P_{vapor} = 1,000 bars Nickel-nickel oxide buffer		
82	QPS	391	360	FPh+FSa+Q+(Cel?)
81	Cel	414	360	FPh?+Cel
71	Cel	420	165	Cel
91	Cel	425	820	FPh+FSa+Q+[Cel]
		Quartz-fayalite-magnetite buffer		
96	QPS	386	700	Cel+[FBt+FSa+Q]
83	Cel	418	360	FBt?+Q+[Cel?]

(SQL). All three were grown from a glass of the composition $K_2O \cdot 2MgO \cdot Fe_2O_3 \cdot 8SiO_2$, which was prepared in the manner discussed earlier.

The celadonite bulk composition yields three different assemblages:

(a) celadonite (low temperature, high and low f_{O_2}),
(b) ferriphlogopite+ferrisanidine+quartz (high temperature and high f_{O_2}), and
(c) ferribiotite+quartz+glass (high temperature and low f_{O_2}).

They are related by the following three reactions:

(1) $MgFe^{3+}$-celadonite$\rightleftarrows Fe^{3+}$-phlogopite+Fe^{3+}-sanidine+quartz+vapor
(2) $MgFe^{3+}$-celadonite$\rightleftarrows Fe^{3+}$-biotite+quartz+liquid+vapor
(3) Fe^{3+}-biotite+Fe^{3+}-sanidine+quartz$\rightleftarrows Fe^{3+}$-biotite+quartz+liquid+vapor

Equilibrium temperatures for reaction (1) were determined using the (HM) and (NNO) buffers, and reaction, (2), using the (QFM) and (IM) buffers. On the (HM) buffer the equilibrium temperature lies between 424° C. (exp. 72, Table 8) and 439° C. (exp. 75), while on the (NNO) buffer the equilibrium temperature is above 405° (exp. 50) and possibly above 417° C. (exp. 32).

The equilibrium temperature of reaction (2) on the (QFM) buffer is between 418° (exp. 66) and 412° (exp. 63). On the (IM) buffer it is between 402° C. (exp. 33) and 392° (exp. 65). In order to make extrapolations possible the temperature limits quoted above have been plotted on a 1/T versus log P plot (Fig. 13). Phase boundaries represented by the reactions (1), (2) and (3) must merge in an isobaric invariant point. This

TABLE 9. POINTS LOCATED BY EXTRAPOLATION OF RUN DATA ON FIG. 10
P_{tot} = 2,000 bars

Reaction	Buffer	Equilibrium Temp., °C	log f_{O_2}, atm.
(1)	HM	431°±7°	−21.0±0.5
(1)	NNO	420°±10°	−26.8±0.6
(2)	QFM	414°±4°	−29.7±0.3
(2)	IM	398°±5°	−34.8±0.6
	Invariant point	416°±5°	−28.8±0.5

geometric requirement narrows the possible temperature ranges considerably. Extrapolated values with probable limits of error have been summarized in Table 9.

Reaction (2) was reversed by growing celadonite from a ferriphlogopite +ferrisanidine+quartz assemblage rather than from ferribiotite+quartz +glass. This is permissible because ferrisanidine melts quickly and probably before celadonite has a chance to grow (Tables 11, 8). The phase boundary representing reaction (3) must lie between the f_{O_2}-T curves for the QFM and NNO buffers. This can be deduced from the fact that celadonite decomposes to ferriphlogopite+ferrisanidine+quartz at the f_{O_2} of the NNO buffer (exp. 24, 26, 39) and to ferribiotite+quartz +glass at the f_{O_2} of the QFM buffer (exp. 35, 97). To verify this conclusion, ferribiotite+quartz+liquid was grown from synthetic celadonite on the IM buffer at 500° C. (same conditions as exp. 98) and then the unopened platinum tube was transferred to an NNO buffer and held at 500° C., for four days (exp. 106). The products were indeed ferriphlogopite+ferrisanidine+quartz.

Mention should be made of the problem concerning the change of composition of the ferribiotite as the value of f_{O_2} is decreased. On the

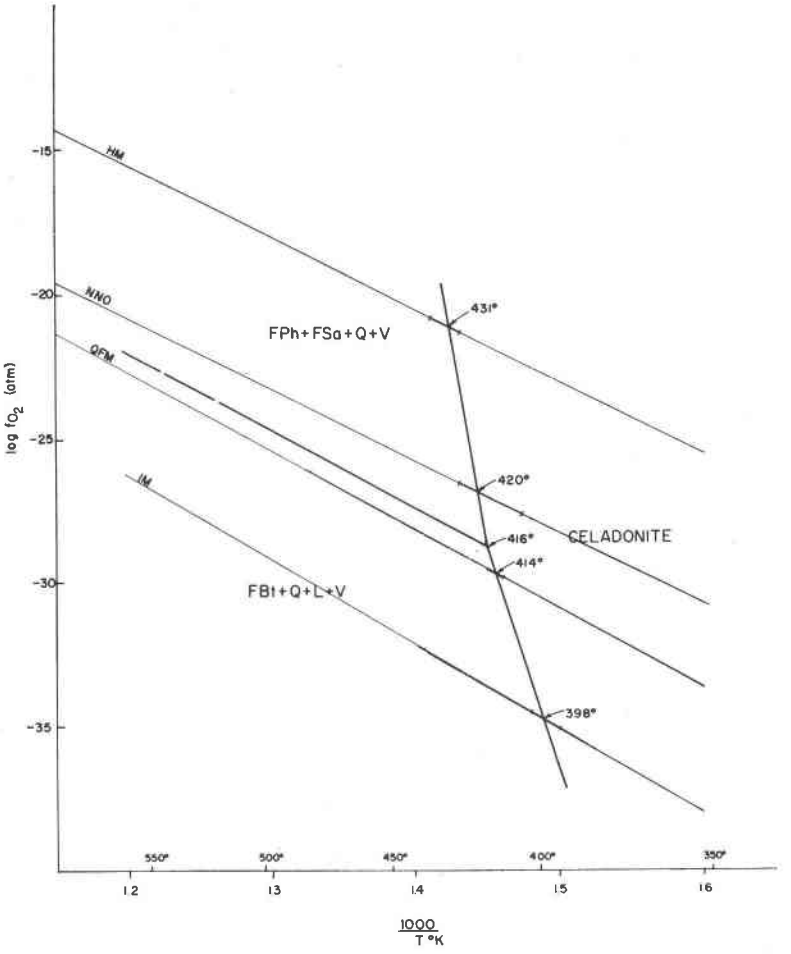

FIG. 13. log f_{O_2}-1/Tω plot, indicating temperature intervals between the lowest temperature at which celadonite was broken down and the highest temperature at which the reaction was reversed. The temperatures shown are the graphical interpolations.

(HM) and probably on the (NNO) buffers the composition is near ferriphlogopite. On the (QFM) buffer nearly $\frac{1}{3}$ of the octahedral sites are filled with ferrous iron. Since the ferribiotites probably form a continuous solid solution series, the composition of the ferribiotites must be identical on each side of the phase boundary representing reaction (3). The use of the term "ferriphlogopite" in the high-f_{O_2} field and of "ferribiotite" in the low-f_{O_2} field is not to imply a discontinuity in composition along phase boundary (3).

Four experiments were run at 1,000 bars total pressure, using the (NNO) buffer. Reaction rates were found to be exceedingly slow. However, probable reaction reversals give an equilibrium temperature of 403° ±8° C. for reaction (1).

From the 2,000 bar section and the 1,000 bar point it is possible to construct a P_{vapor}-T diagram (Fig. 14). By plotting log P_{vapor} *vs.* 1/T (Fig. 15), it is possible to arrive at an approximate value for the enthalpy change for reaction (1). ΔH was found to be 51 Kcal/mole, a value similar to those of other decomposition reactions involving micas (Yoder and Eugster, 1954, 1955).

The reactions controlling the stability of celadonite can be schematically represented on a triangular diagram with (Mg, Fe)O, Fe_2O_3, and SiO_2 at the apices. All phases are projected from the H_2O and K_2O corners. In Fig. 16a reaction (1) is represented by a triangle, FBt+FSa +Qz, with the celadonite bulk composition lying within this triangle. However, when f_{O_2} is lowered (in reactions 2 and 3) the bulk composition changes along the line shown in Fig. 16b, since the Fe_2O_3 content is being reduced. Ferrisanidine is no longer stable, and the bulk composition of the celadonite system must lie within the triangle, FBt+Qz+L. Reaction (3) is characterized by the melting of ferrisanidine to ferribiotite +liquid+oxygen. Again, the bulk composition shifts to the triangle, FBt+Qz+L.

Synthesis of other celadonite end members. The four end members of tetrasilicic celadonites were previously discussed. It was also pointed out that the compositions of most natural celadonites can only be expressed when muscovite and ferrimuscovite are used as additional end members. Figure 17 is a prism which represents most of the celadonite end members. On the base are the tetrasilicic end members, and on the upper edge the series muscovite-ferrimuscovite. The compositions of various celadonites, whose synthesis was attempted, are given by circles. Synthetic celadonites were obtained only along the join $Fe^{2+}Fe^{3+}$-celadonite–$MgFe^{3+}$-celadonite.

Results of experiments are given in Table 10.

The $Fe^{2+}Fe^{3+}$-celadonite was grown from a reduced glass of the composition, $K_2O \cdot 4Fe \cdot 8SiO_2$, at 306° (exp. 78). The glass at higher temperatures produced ferriannite and quartz according to the reaction:

$$(K_2O \cdot 4Fe \cdot 8SiO_2) + 2\tfrac{1}{4}O_2 + H_2O \rightleftarrows KFe_3^{2+}Fe^{3+}Si_3O_{10}(OH)_2 + 5SiO_2 + (\tfrac{1}{2}K_2O).$$

A condensed phase containing the excess potash was not found. The (060) reflection of the $Fe^{2+}Fe^{3+}$-celadonite has a d-spacing of 1.530 Å, as compared to 1.512 Å for the $MgFe^{3+}$-celadonite. This change is similar and

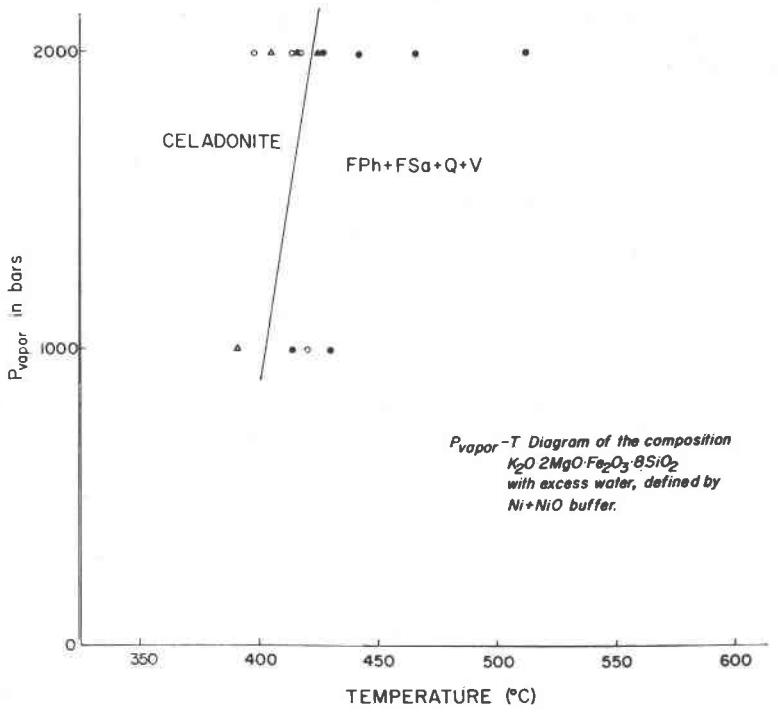

FIG. 14. P_{vapor}-T diagram of the composition $K_2O \cdot 2MgO \cdot Fe_2O_3 \cdot 8SiO$ with excess water and defined by the Ni+NiO buffer. Symbols used are the same as those in Fig. 12.

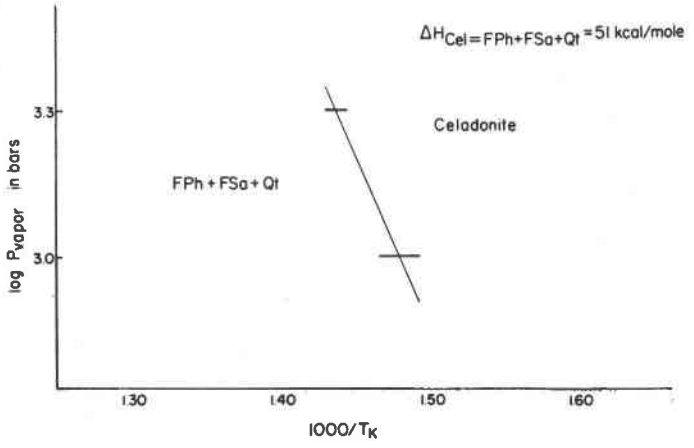

FIG. 15. log P_{vapor}-$1/T_K$ plot of the relations given in Fig. 14.

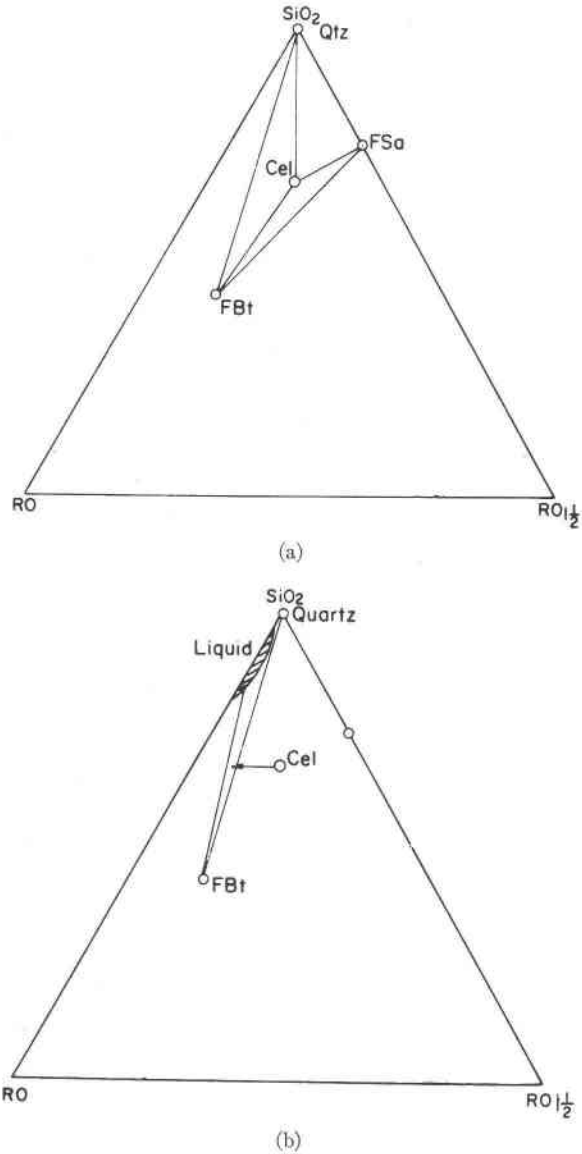

FIG. 16. Schematic representation of the three reactions governing the celadonite stability. The phases are represented on the triangular diagrams—SiO_2–RO–$RO_{1\frac{1}{2}}$, in which RO represents MgO and FeO, and $RO_{1\frac{1}{2}}$ is Fe_2O_3. Phase compositions are projected from the K_2O and H_2O apices. Reaction 1 (Cel$\rightleftharpoons$FSa+FBt+Qtz) is represented by Fig. 16a. Here RO is MgO only. Reaction 2 (Cel$\rightleftharpoons$FBt+Qtz+liquid) is represented by Fig. 16b. Here the bulk composition shifts with a loss of oxygen to a point within the triangle FBt-Qtz-liquid. RO is MgO plus some FeO. Reaction 3 (FSa$\rightleftharpoons$FBt+liquid) is represented by the two diagrams. Again in this reaction the bulk composition changes to a point within the triangle FBt-Qtz-liquid with the loss of oxygen.

on the same order of magnitude as those of the biotite series. (See, for example, the (060) values for ferriphlogopite and ferriannite, Table 7.) The mean refractive index for $Fe^{2+}Fe^{3+}$-celadonite is 1.615.

Three celadonites along the join $MgFe^{3+}$-celadonite-$Fe^{2+}Fe^{3+}$-celadonite (compositions 10, 11, and 12 in Fig. 17) were grown from mixtures of reduced glasses. These celadonites (exps. 87, 88, and 89) all have $d_{(060)}$

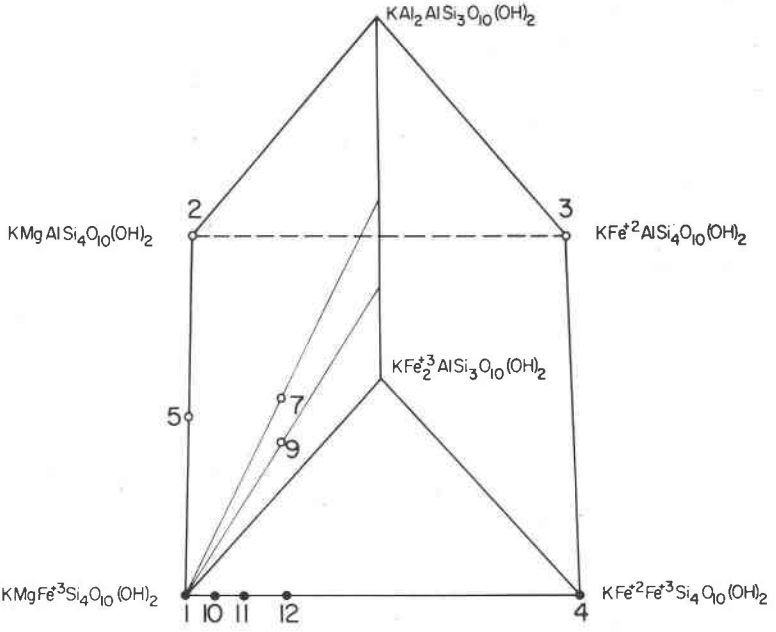

FIG. 17. Compositional prism representing the compositions of most celadonites. The base of the prism represents the tetrasilicic celadonite end members, while the apices represent the muscovite-ferrimuscovite series. Solid circles give the compositions of the celadonites that have been synthesized; the open circles, no mineral with the celadonite structure has been made.

and N_m values (1.514 Å and 1.620, respectively) similar to those of $MgFe^{3+}$-celadonite grown near the same f_{O_2} (exp. 51).

A mix of the composition $KMgAlSi_4O_{10}$ (no. 2, Fig. 17) was prepared from a $K_2O \cdot 8SiO_2$ glass, MgO, and γ-Al_2O_3. Runs with this mix invariably produced phlogopite, sanidine and quartz, even when seeded with celadonite.

A mix of the compositions $KFe^{2+}AlSi_4O_{10}$ (no. 3, Fig. 17) was prepared from a $K_2O \cdot 8SiO_2$ glass, ferrous oxalate, and γ-Al_2O_3. A celadonite of this composition was never obtained, and run products always contained siderite.

TABLE 10. RUN DATA FROM THE EXPERIMENTS ON CELADONITE END MEMBERS (COMPOSITIONS ARE ILLUSTRATED IN FIG. 17)

Abbreviations:

Cel	celadonite
FPh	ferri-phlogopite
FSa	ferri-sanidine
Q	quartz
Sa	sanidine
Phl	phlogopite
Musc	muscovite
Mag	magnetite
FAn	ferri-annite
(Spl)	tube containing the charge was found split; the phases remaining are given.
( )	questionable identification

Temp. (°C)	P_{vapor} (bars)	Time (hrs.)	Buffer	Condensed Phases
		(1) $K_2O \cdot 2MgO \cdot Fe_2O_3 \cdot 8SiO_2$ (glass)		
296	2,000	160	—	Cel
339	2,000	145	—	Cel
355	2,000	2,100	—	Cel
402	2,000	162	—	Cel
444	2,000	501	—	Cel
494	2,000	160	—	FPh+FSa+Q
595	2,000	143	—	FPh+FSa+Q
		(2) $K_2O \cdot 2MgO \cdot Al_2O_3 \cdot 8SiO_2$ (mix)		
306	2,000	136	—	Q+Sa+(Phl?)
355	2,000	2,100	—	Sa+Phl+Q
400	2,000	164	—	Q+Sa+(Phl?)
450	2,000	160	—	(spl)−Q+Sa+Phl
500	2,000	1,800	—	Phl+Sa+Q
600	2,000	1,800	—	Phl+Sa+Q
650	2,000	1,800	—	Phl+Sa+Q
		(3) $K_2O \cdot 2FeO \cdot Al_2O_3 \cdot 8SiO_2$ (mix)		
306	2,000	136	—	siderite+Sa+Q
400	2,000	164	—	Sa+Musc+Mag
450	2,000	160	—	Q+annite
		(4) $K_2O \cdot 2FeO \cdot Fe_2O_3 \cdot 8SiO_2$ (mix)		
306	2,000	136	—	Fan+siderite+Q
400	2,000	164	—	Mag+Q+(FAn?)
450	2,000	160	—	(spl)−Mag
500	2,000	162	—	(spl)−Mag+FAn
		(4) $K_2O \cdot 3Fe \cdot 8SiO_2$ (reduced glass)		
306	2,000	190	—	Cel+Q
343	2,000	290	NNO	Cel or FAn (no 060 peak on *x*-ray pattern)

TABLE 10—(*Continued*)

Temp. (°C)	P_{vapor} (bars)	Time (hrs.)	Buffer	Condensed Phases
376	2,000	270	—	Q+FAn
391	2,000	165	—	Q+FAn
	(5) $2K_2O \cdot 4MgO \cdot Fe_2O_3 \cdot Al_2O_3 \cdot 16SiO_2$ (glass)			
291	2,000	312	—	Q+San+Cel
401	2,000	165	—	Q+San+Cel
557	2,000	145	—	Q+FPh+San
	(7) $2K_2O \cdot 2MgO \cdot 2Fe_2O_3 \cdot Al_2O_3 \cdot 14SiO_2$ (glass)			
306	2,000	190	—	Q+Sa+Cel
376	2,000	270	—	Sa+hematite
391	2,000	165	—	Q+Sa+(Cel?)

A glass with the composition of the point midway on the join between the $KMgFe^{3+}Si_4O_{10}$ and $KMgAlSi_4O_{10}$ end members (point 5, Fig. 17) yielded the following products: $MgFe^{3+}$-celadonite, phlogopite, sanidine, and quartz. It was concluded from these experiments that large amounts of aluminum were not stable in the octahedral positions of the synthetic celadonites. The significant amounts in the natural celadonites and glauconites may arise from solid solutions or mixed layering with montmorillonites and illites (Hower, 1961).

Attempts were made to synthesize celadonites (or glauconites) with compositions between the $MgFe^{3+}$-celadonite and the muscovite-ferrimuscovite series (points 7 and 9, Fig. 17), but the results are largely inconclusive.

The stability of ferrisanidine. Ferrisanidine is an important phase in the high temperature assemblages of $MgFe^{3+}$-celadonite bulk composition. A few preliminary experiments were run to outline the general stability field of this phase at 2,000 bars total pressure (Table 11).

The high temperature-low f_{O_2} phases below the HM buffer are ferriannite ($KFe_3^{2+}Fe^{3+}Si_3O_{10}(OH)_2$ (B) and one or two liquids, that is, ferrisanidine melts incongruently according to the reaction

$$\underset{\text{FS}}{4KFe^{3+}Si_3O_8} \rightleftarrows \underset{\text{B}}{KFe_3^{2+}Fe^{3+}Si_3O_{10}(OH)_2} + \text{liquid } (K_2O \cdot xSiO_2 \cdot yFeO \cdot zFe_2O_3) \qquad (4)$$

On the IM buffer (point I) the temperature for this reaction lies at 437 ±17° C. (exp. 76 and 95, Table 11). On the NNO buffer ferrisanidine melted at 637° C. (exp. 103) and ferrisanidine grew from ferriannite +glass at 597° C. (exp. 102). Point H was, therefore, placed at 616° ±20° C. On the QFM buffer ferrisanidine was grown from ferriannite +glass at 452° C. (exp. 112); it melted to ferriannite+liquid at 735° C.

(exp. 100) and remained unchanged in a short run at 593° C. (exp. 104). A few experiments performed at the HM buffer apparently did not yield equilibrium assemblages (Wones, 1963).

TABLE 11. TABLE OF EXPERIMENTAL RESULTS OF RUNS WITH BULK COMPOSITION $K_2O \cdot Fe_2O_3 \cdot 6SiC_2$ AT 2,000 BARS TOTAL PRESSURE

Abbreviations used:
Fsa —ferrisanidine
FAn —ferriannite ( )—phase unstable
FMi —ferrimicrocline
r-glass —reduced glass
FAn+G—ferriannite plus glass
Mt? —questionable magnetite phase
Q —quartz
L —Liquid (numbers indicate more than one liquid)

Exp. No.	Starting Material	Temp. °C.	Time hrs.	Condensed phases
		Hematite-magnetite buffer		
110	FAn+G	655	70	FSa
114	FAn+G	703	60	(FAn+L)
115	FAn+G	763	60	(FAn+L)
		Nickel-Nickel oxide buffer		
111	FAn+G	463	90	FSa
102	FAn+G	597	70	FSa
108	FAn+G	620	90	FAn+L
103	FSa	637	95	FAn+L
101	FAn+G	678	70	FAn+L
99	FSa	735	75	FAn+L_1+L_2
		Quartz-fayalite-magnetite buffer		
112	FAn+G	452	90	FSa+(FAn+L)
77	r-glass	578	260	FAn+L
104	FSa	593	95	FSa
100	FSa	735	70	FAn+L
		Magnetite-iron buffer		
76	r-glass	420	285	FAn+FMi+Mt? Q
113	FAn+G	453	90	FAn+L
95	FSa	455	170	FAn+L
93	r-glass	471	310	FAn+Q+L
94	r-glass	553	310	FAn+L
		Wusite-iron buffer		
86	r-glass	647	165	FAn+L
105	FSa	736	95	FAn+L_1+L_2

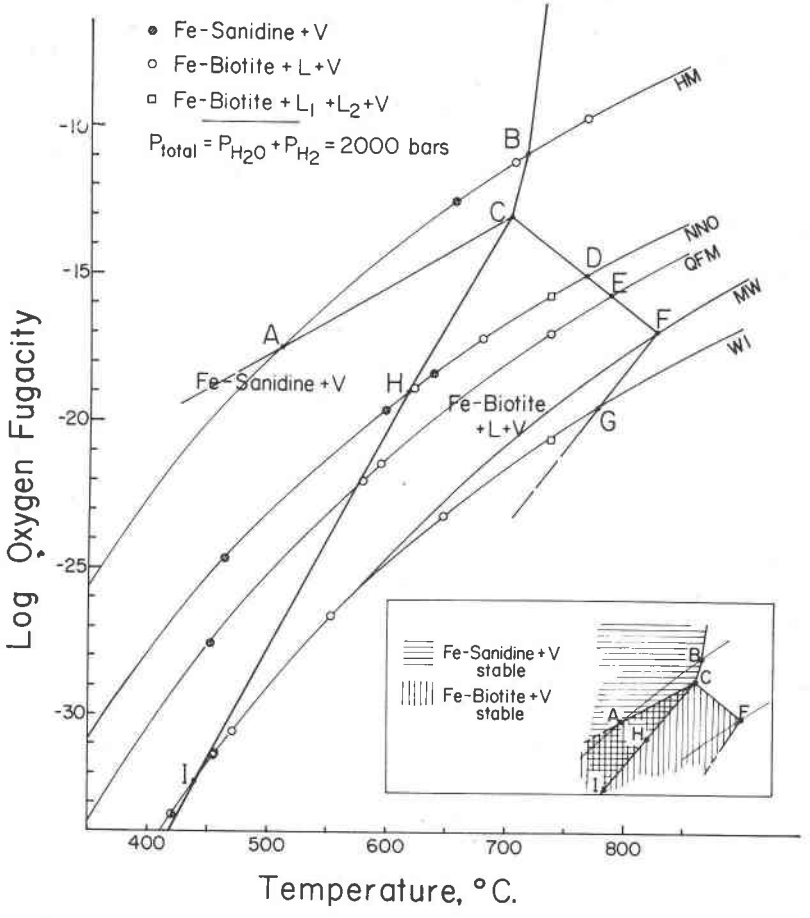

FIG. 18. f_{O_2}-T section at 2,000 bars total pressure for the bulk composition $K_2O \cdot Fe_2O_3 \cdot 6SiO_2$. Abbreviations are listed in Table 11.

These very preliminary and incomplete data on the stability of ferrisanidine at 2,000 bars have been combined in Fig. 18 with the data of Wones (1963) on the stability of ferriannite. Ferrisanidine is stable to the left of curve IHCB. It melts to ferriannite+liquid along the line IHC. The composition of the liquid formed changes as a function of temperature and f_{O_2}, as indicated by the refractive index of the glass formed. At low temperatures a colorless glass with n=1.52 was obtained. At higher temperatures the glass is pale blue or gray with n=1.55. At the highest temperatures on the WI buffer (exp. 105) two liquids probably formed, because glasses with two refractive indices: n=1.540 and n=1.545 (one is

gray and the other is green, respectively) were observed. The intersection of the line HC with the QFM buffer curve is not well known, but must lie above 452° C. Along the line CB ferrisanidine melts to magnetite+liquid. Wones (1963) found point B to be at 715° C. Point C, which is at the intersection of curves IH and FED must be close to 700° C. and $f_{O_2} = 10^{-13}$ atm. Above point B ferrisanidine melts to hematite+liquid. It is inter-

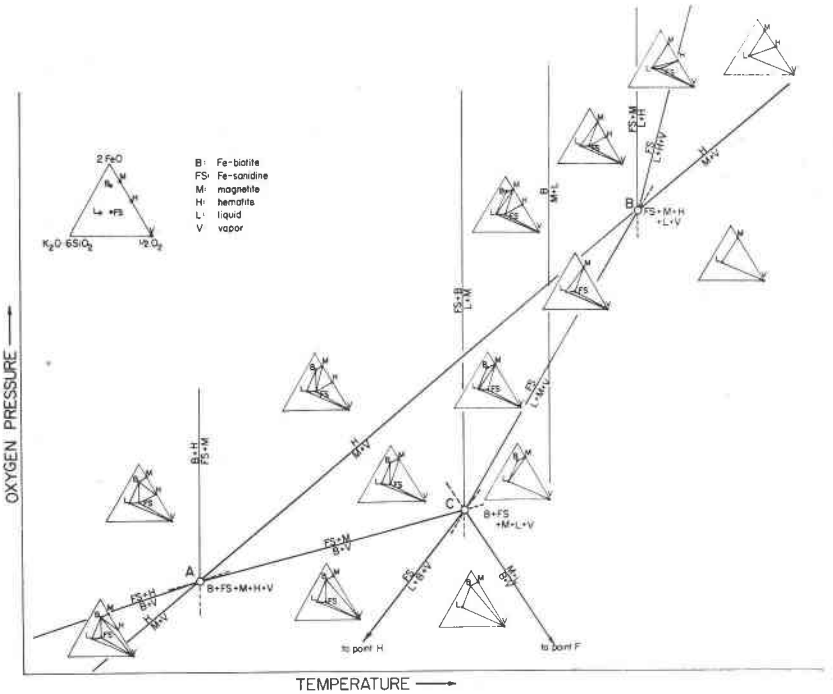

FIG. 19. Oxygen pressure-temperature diagram, illustrating reactions in the region around points A, B, and C of Fig. 18.

esting to note that for celadonite bulk composition ($K_2O \cdot 2MgO \cdot Fe_2O_3 \cdot 8SiO_2$) the curve representing the melting of ferrisanidine (Fig. 11 and reaction 3, p. 1057) lies above the QFM buffer curve at temperatures as low as 416° C., that is ferrisanidine at a fixed P_{O_2} melts at a lower temperature for celadonite bulk composition than from its own bulk composition. This of course is as it should be.

Figure 18 also shows the stability field for ferriannite, as determined by Wones (1963). Ferriannite is stable below curve AC and to the left of curves CDEF and FG.

Phase relations in the vicinity of points A, B, and C have been analyzed completely in Fig. 19, for a constant P_{H_2O} of 2,000 bars, with H_2O pres-

ent in excess. The compositions of all six phases encountered: Fe-biotite (B), Fe-sanidine (FS), magnetite (M), hematite (H), melt (L) and vapor (V) can be represented by the four components $K_2O \cdot 6SiO_2$, 2FeO, H_2O and O_2. They are shown in Fig. 19 on the base of the tetrahedron, projected from the H_2O apex. A, B and C are (isobaric) invariant points with five univariant curves radiating from each point. Three of the curves, one from each invariant point, involve condensed phases only.[1] Two curves each for points A and B are identical with the HM buffer curve. The remaining two curves from Point A represent the decomposition of Fe-biotite and the remaining two curves from point B represent the incongruent melting of Fe-sanidine. The remaining four curves from point C represent respectively the melting of Fe-sanidine to Fe-biotite +liquid, the melting of Fe-sanidine to magnetite+liquid, the melting of Fe-biotite to magnetite+liquid and the decomposition of Fe-biotite to Fe-sanidine+magnetite. All possible phase assemblages within a given f_{O_2}-T field for bulk compositions within the MBLV area are shown graphically in Fig. 19. The composition of V as shown in Fig. 19 is nearly pure oxygen, though the actual vapor involved will be a mixture of $H_2O+H_2+O_2$, as defined by the specific f_{O_2} involved. The composition of L is not strictly constant, but its general location is defined by the relative location of the reaction curves shown in Fig. 18. Positions of metastable extensions can be derived from the number of assemblages which must be stable in each f_{O_2}-T area. Several joins shown in Fig. 19 are not stable in the presence of an oxygen-bearing vapor and therefore are not encountered in hydrothermal experiments.

Geologic Applications

At a vapor pressure of 2,000 bars the $MgFe^{3+}$-celadonite is stable to temperatures slightly higher than 400° C. (Table 9). Variations in f_{O_2} have little effect on this temperature. As mentioned earlier celadonite is a mineral of the zeolitic facies and has not been reported for mineral assemblages of the greenschist facies. It is obvious, therefore, that natural celadonite disappears during progressive metamorphism long before its upper stability limit has been reached. This is also indicated by the breakdown products of pure celadonite: ferriphlogopite and ferrisanidine, neither of which is an important mineral.

The ideal composition of minerals commonly associated with cela-

[1] The existence of a fourth curve between condensed phases alone must be postulated at $T_B > T > T_C$ for the reaction biotite$\rightleftharpoons$magnetite+liquid. This reaction is necessary to properly separate bivariant regions between points B and C. The composition of the liquid of course is somewhat different from the point L assumed in Fig. 18. This curve is not stable in the presence of an oxygen bearing vapor.

donites can be plotted in a triangular diagram with $(Al_2O_3+Fe_2O_3)$, $(MgO+FeO)$ and K_2O as apices. SiO_2 and H_2O are assumed to be present in excess, CaO is at first considered to be absent and will be added later. Figure 20 shows part of this triangle. Only minerals commonly associated with celadonite are plotted. The sequence of reactions which will be encountered during progressive metamorphism is difficult to predict because of the lack of relevant data on natural minerals and mineral assemblages and on synthetic systems. It is, nevertheless, useful to dis-

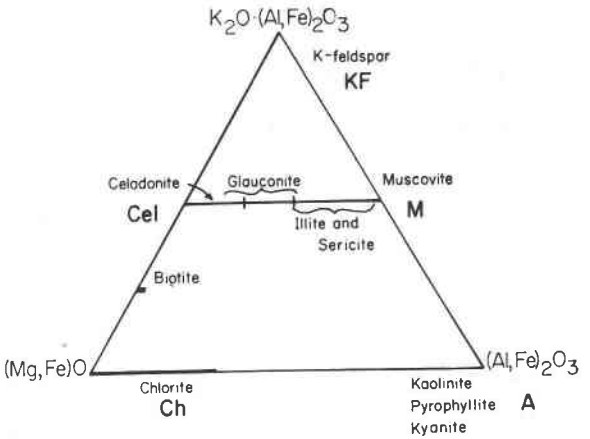

FIG. 20. The triangular plot of K_2O-$(Al,Fe)_2O_3$, $(Mg,Fe)O$, and $(Al,Fe)_2O_3$, showing the minerals that can be expressed with these components, assuming excess SiO_2 and H_2O.

cuss a probable path, though this path may later have to be modified in the light of new data. Figure 21 shows such a path which is based on several assumptions, some of which are discussed below.

The following reactions have been assumed to take place with increasing temperature at a constant water pressure:

I. Celadonite+hydrous aluminous silicate⇌muscovite+chlorite
II. Celadonite+muscovite+potash feldspar
V. Celadonite+chlorite⇌biotite[1]
VI. Celadonite⇌biotite+potash feldspar
VII. Chlorite+potash feldspar⇌biotite+muscovite
VIII. Chlorite+muscovite⇌biotite+aluminous silicate

of these reactions only reaction VI has been investigated experimentally (this paper); the others were inferred from natural assemblages.

[1] Reactions III and IV appear in Fig. 22. They do not involve celadonite.

The existence of reaction I, which most likely is the reaction by which the bulk of celadonite disappears during progressive metamorphism, depends upon the relationship between celadonite, glauconite and muscovite. The extent of solid solution (by ionic substitution or by mixed layering) along the celadonite-muscovite joint is not known. As mentioned previously the number of silicon atoms per 12 (O, OH, F) varies in celadonites between 4.0 and 3.70 and in glauconites between 3.8 and 3.4, while some illites (Deer *et al.*, 192, p. 218–220) contain as much as 3.5

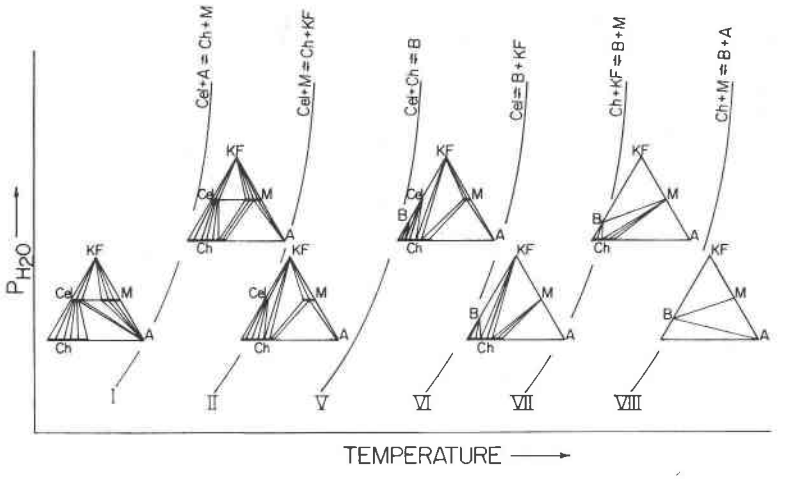

FIG. 21. P_{H_2O}-T diagram to illustrate the participation of celadonite in certain proposed metamorphic reactions. See text for discussion. The symbols are those used in Fig. 20.

Si. In the case of the illites, in particular, high Si values may be caused either by admixed silica (too fine-grained to appear on *x*-ray powder patterns) or by mixed-layering with montmorillonite.

The extent of solid solution between glauconites and muscovites is uncertain, although a fair number of good glauconite analyses are available (see Owens and Minard, 1960). Burst (1958) demonstrated that many glauconite pellets are actually mixtures of glauconite with illite, montmorillonite, chlorite and other minerals. Separation of phases is often impossible and many reported chemical analyses may have been performed on mixtures.

The existence of muscovites with high silica contents seems to be well established. Examples have been reported for instance by Schaller (1950) and by Lambert (1959). Discounting old analyses and analyses performed on impure material (analyses of mariposite, alurgite and leucophyllite, see Schaller, 1950), such muscovites seem to be able to contain as much

as 3.45 silicon atoms per 12 (O, OH, F). They appear to lie close to the muscovite ($KAl_2AlSi_3O_{10}(OH)_2$)—leucophyllite ($KAlMgSi_4O_{10}(OH)_2$) join and are commonly called phengites. All reliable phengite analyses lie closer to muscovite than to leucophyllite. Attempts at synthesis of the end member leucophyllite over a range of temperatures have yielded phlogopite as the only micaceous phase. It is important to note that most well documented high-silica muscovites and phengites come from metamorphic or hydrothermal environments. Furthermore, Lambert (1959) found a tendency for the silica content to decrease with increasing grade of metamorphism.

In summary, it is possible to find analyses to cover the whole range of Si:Al ratios between muscovite and celadonite. However, if purely sedimentary environments (most glauconites) are excluded, there appears to be a break between about 3.45 and 3.70 silicon atoms per half unit cell. This break has been assumed to exist in Fig. 21 for celadonite assemblages of the lowest metamorphic grade.

Celadonites commonly are associated with clay minerals such as montmorillonite. Therefore the join celadonite-hydrous aluminous silicate (A) has been assumed to be stable rather than the join muscovite-chlorite at the beginning of incipient metamorphism.[1] If this assumption is correct, the following three-phase assemblages should exist:

Celadonite+chlorite+aluminous silicate
Celadonite+muscovite+aluminous silicate

The first assemblage has been observed, but no celadonite-muscovite assemblages have so far been reported except for possible glauconite, illite, and montmorillonite assemblages in glauconite pellets. There seems to be no obvious reason why this pair should not coexist. However, very careful work would be required to detect the presence of both micas in fine-grained mixtures. It is also possible that the compositional requirements are not commnly met for this pair to form.

The first reaction assumed to take place on rising temperatures (or decreasing P_{H_2O}) is that between celadonite and the aluminous silicate, with an excess of SiO_2 and H_2O present:

(I) celadonite+aluminous silicate$\rightleftarrows$muscovite+chlorite

[1] As was pointed out by Thompson (1957), MgO and FeO can, in most instances, not be treated as one component. If they are, as in Fig. 21, joins may cross, even for fixed values of P_{H_2O} and T. The coexistence of celadonite and montmorillonite, for instances, does not preclude the coexistence of muscovite with a chlorite, whose MgO/FeO ratio is significantly different from that of celadonite. For the same reason, univarient reactions shown in Fig. 21 are in reality families of reactions, occupying P_{H_2O}-T regions. These objections, however, do not invalidate the usefulness of Figs. 21 and 22, which must be regarded as very crude first attempts at illustrating an exceedingly complex group of problems.

This reaction has not yet been observed in the field or in the laboratory. If it does take place as indicated, it could be a most significant step during incipient metamorphism, since it could represent the first appearance of metamorphic muscovite. If illite was present in the original sediment, the reaction must be detected by the disappearance of celadonite or kaolinite rather than by the appearance of muscovite.

Reaction I marks the disappearance of celadonites from all those celadonite assemblages, whose bulk composition lies on the Al_2O_3-rich side of the muscovite-chlorite join.

The next reaction assumed to take place is:

(II) celadonite+muscovite⇌chlorite+potash feldspar which creates the following assemblages:

celadonite+chlorite+potash feldspar
chlorite+muscovite+potash feldspar
chlorite+muscovite+aluminous silicate

The first assemblage has been observed in some celadonite-bearing rocks, although the potash feldspar is usually present only in the norm, since the accompanying zeolite contains some potassium. The other two assemblages of course are typical for low-grade slates and schists. The reaction observed by Dickinson (1962) is perhaps of this type.

The next step could be the appearance of biotite at the expense of celadonite and chlorite:

(V) celadonite+chlorite⇌biotite

The chlorite participating in this reaction is less aluminous than the chlorites which coexist with celadonite+potash feldspar and with muscovite.

So far each successive reaction has decreased the range of bulk compositions for which celadonite is a stable phase. The next reaction represents the upper stability limit of pure celadonite and it is the reaction investigated in this paper:

(VI) celadonite⇌biotite+potash feldspar

Above this reaction celadonite should not be present in mineral assemblages for any bulk composition.

Two additional reactions have been indicated in Fig. 21:

(VII) chlorite+potash feldspar⇌muscovite+biotite
(VIII) chlorite+muscovite⇌biotite+aluminous silicate

The retrograde equivalent of reaction VII has been described by Chayes (1955) and reaction VIII could be the equivalent of the kyanite or garnet isograd, depending upon the bulk composition.

A shortcoming of Fig. 21, as pointed out by D.S. Coombs (pers. communication) is the omission of two minerals—saponite and stilpnomelane. Coombs (pers. comm.) says that "stilpnomelane appears freely long before biotite in New Zealand and elsewhere." Coombs also believes that "reactions including loss of stilpnomelane are important in the production of biotite at the onset of the biotite zone." Recent studies involving stilpnomelane and stilpnomelane-bearing assemblages have been made by Blake (1958) and Zen (1960). Blake (1958) found stilpnomelane in iron formations commonly associated with minnesotaite. Zen (1960) pointed out that the stilpnomelane-microcline-chlorite assemblage rules out "the chlorite Fe-biotite pair, which in fact is not found in the area although biotite does occur." Zen (1960, Fig. 5, p. 158) also stressed the fact that in an AKF diagram (equivalent to Figs. 21, 22) apparent crossing the tie-lines is possible for P_{H_2O}-T areas between reaction curves, because of the lumping of FeO and MgO as one component.

No information is available on celadonite-stilpnomelane assemblages. It is conceivable that celadonite could participate in a reaction of the type:

$$\text{celadonite} + \text{chlorite} \rightleftharpoons \text{stilpnomelane}$$

Saponite, only provisionally reported (Ross, 1958; Wise, 1961) may be replaced by chlorite very early. Far more data are needed in order to evaluate the role of saponitic clays. However, until more information becomes available, Fig. 21 still is useful in its present incomplete form.

Most celadonite assemblages are found in an environment rich in CaO as well as alumina. Heulandite is the most common calcic mineral associated with celadonite (Coombs *et al.*, 1958; Wise, 1961) calcite+celadonite is quite common (Wise, 1961) and laumontite+celadonite (Coombs *et al.*, 1959) as well as clinoptilolite+celadonite (Coombs, 1958; Hay, 1962, 1963; Fisher, 1963) have also been reported. The most extensive summary of zeolite reactions inferred from natural assemblages and from laboratory studies is that of Coombs *et al.* (1959). Zen (1961) has pointed out the relationship between zeolite and carbonate assemblages. He concludes that:

". . . it appears that at constant temperature and pressure, it is possible to obtain, for a system isochemical with respect to the inert components, both mineral assemblages characteristic of the zeolite facies and of the greenschist facies, depending on the relative values of μ_{H_2O} and μ_{CO_2}. At high values of μ_{H_2O} and low values of μ_{CO_2} the zeolite facies prevails; however, many sediments and sedimentary rocks evidently did not crystalize under these conditions. Relative values of μ_{CO_2} are commonly high enough so that the alternative assemblages, calcite-kaolinite-quartz or calcite-pyropyllite-quartz, obtain."

To include celadonite-bearing assemblages, Zen's treatment must be extended by adding both (Mg, Fe)O and K_2O. This amounts to adding CaO and CO_2 to Fig. 21. A schematic analysis of the most probable se-

quence of mineral reactions and mineral assemblages is shown in Fig. 22, which is a μ_{H_2O}-μ_{CO_2} plot drawn at constant temperature and constant total pressure, assuming that SiO_2 and H_2O are present in excess. All reactions which are dehydration-hydration reactions only lie on lines parallel to the μ_{CO_2} axis. Reactions involving transfer of both CO_2 and H_2O proceed along lines inclined to both axes. The slopes can be calculated from the mole fractions of the participating gases (see, for instance, Zen, 1961), but only if the solids involved have a fixed and known composition. In the case at hand it is possible to show relative slopes only.

It should be pointed out that the sequence of reactions from the top to the bottom of Fig. 22 is also the sequence to be expected with rising temperature, and temperature differences are probably involved in most cases when such a sequence is observed in nature.

The basic mineral configuration of Fig. 22 is a simplified version of Fig. 21 with celadonite, muscovite, biotite, chlorite, potash feldspar and hydrous aluminous silicate (A) all lying in the same plane and with calcite forming the apex of a four-sided pyramid. Solids are treated as if they had a fixed composition and are arranged in such a manner as to permit proper crossing of joins. The problem of the stability of aluminous silicates (kaolinite, montmorillonite, pyrophyllite, etc.) is not considered and A simply stands for any hydrous aluminous silicate. Heulandite, laumontite and prehnite lie in the front face of the pyramid on the A-Cc join. It must be remembered that the pyramid is drawn perspectively in Fig. 21 and that joins which appear to cross on paper do not cross in space.

The basic framework for Fig. 22 is given by reactions I, II, V, VI, which follow each other at successively lower values of μ_{H_2O}. Two additional dehydration reactions must now be considered:

III heulandite$\rightleftharpoons$laumontite+quartz and
IV laumontite$\rightleftharpoons$prehnite+quartz[1]

These two reactions have been placed below the celadonite-muscovite reaction (II) and above the reaction forming biotite (V), because neither celadonite-muscovite nor celadonite-biotite assemblages have so far been reported, while celadonite-heulandite, celadonite-laumontite and celadonite-prehnite assemblages are common. Under different conditions (for instance high load pressure) prehnite might be replaced by lawsonite or zoisite, neither of which has so far been found in association with cela-

[1] Reaction IV is oversimplified in that laumontite can coexist with prehnite over a range of μ_{H_2O} values and is not directly replaced by it, since its CaO/Al_2O_3 ratio differs from that of prehnite. Coombs (1961) has discussed several laumontite-prehnite assemblages and has concluded that "the full sequence of reactions by which first laumontite, then prehnite and pumpellyite are eliminated is not yet clear."

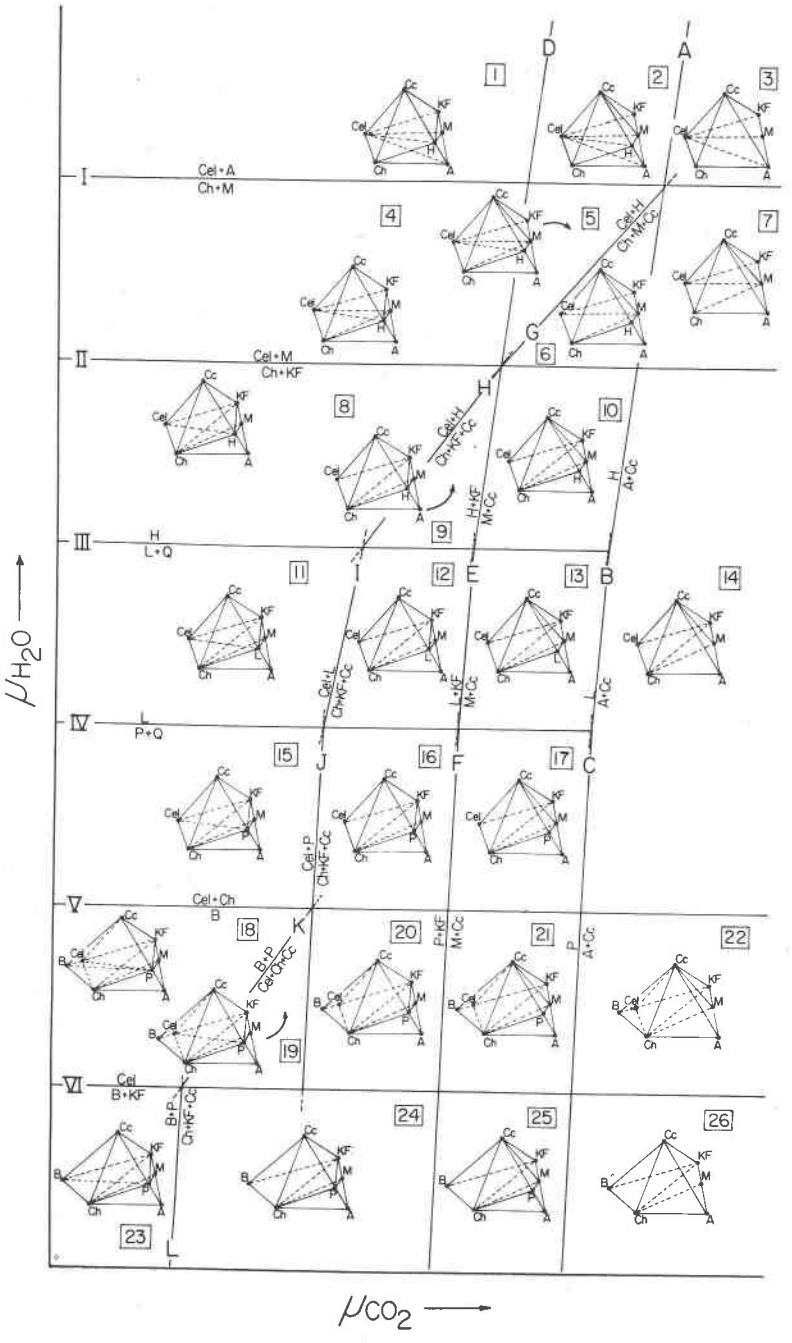

(See legend on facing page)

FIG. 22. μ_{H_2O}-μ_{CO_2} plot drawn at constant temperature and constant total pressure and assuming that SiO_2 and H_2O are present in excess. The possible assemblages for each μ_{H_2O}-μ_{CO_2} field are given below:

		[1] Cel-Ch-A-H Cel-M-A-H Cel-M-KF-H Cel-KF-H-Cc Cel-Ch-H-Cc	[2] Cel-M-KF-Cc Cel-Ch-H-Cc Cel-M-H-Cc Cel-Ch-A-H Cel-M-A-H	[3] Cel-M-KF-Cc Cel-M-A-Cc Cel-Ch-A-Cc
	[4] Cel-KF-H-Cc Cel-Ch-H-Cc Cel-M-KF-H Ch-M-A-H Cel-Ch-M-H	[5] Cel-M-KF-Cc Cel-M-H-Cc Cel-Ch-H-Cc Cel-Ch-M-H Ch-M-A-H	[6] Cel-M-KF-Cc Cel-Ch-M-Cc Ch-M-H-Cc Ch-M-A-H	[7] Cel-M-KF-Cc Cel-Ch-M-Cc Ch-M-A-Cc
	[8] Cel-KF-H-Cc Cel-Ch-H-Cc Cel-Ch-KF-H Ch-M-KF-H Ch-M-A-H	[9] Cel-Ch-KF-Cc Ch-KF-H-Cc Ch-M-KF-H Ch-M-A-H	[10] Cel-Ch-KF-Cc Ch-M-KF-Cc Ch-M-H-Cc Ch-M-A-H	
	[11] Cel-KF-L-Cc Cel-Ch-L-Cc Cel-Ch-KF-L Ch-M-KF-L Ch-M-A-L	[12] Cel-Ch-KF-Cc Ch-KF-L-Cc Ch-M-KF-L Ch-M-A-L	[13] Cel-Ch-KF-Cc Ch-M-KF-Cc Ch-M-L-Cc Ch-M-A-L	[14] Cel-Ch-KF-Cc Ch-M-KF-Cc Ch-M-A-Cc
	[15] Cel-KF-P-Cc Cel-Ch-P-Cc Cel-Ch-KF-P Ch-M-KF-P Ch-M-A-P	[16] Cel-Ch-KF-Cc Ch-KF-P-Cc Ch-M-KF-P Ch-M-A-P	[17] Cel-Ch-KF-Cc Ch-M-KF-Cc Ch-M-P-Cc Ch-M-A-P	
[18] Cel-KF-P-Cc Cel-B-P-Cc Ch-B-P-Cc Cel-B-Ch-P Cel-Ch-KF-P Ch-M-KF-P Ch-M-A-P	[19] Cel-Ch-B-Cc Cel-Ch-P-Cc Cel-KF-P-Cc Cel-Ch-KF-P Ch-M-KF-P Ch-M-A-P	[20] Cel-Ch-B-Cc Cel-Ch-KF-Cc Ch-KF-P-Cc Ch-M-KF-P Ch-M-A-P	[21] Cel-Ch-B-Cc Cel-Ch-KF-Cc Ch-M-KF-Cc Ch-M-P-Cc Ch-M-A-P	[22] Cel-B-Ch-Cc Cel-Ch-KF-Cc Ch-M-KF-Cc Ch-M-A-Cc
[23] B-KF-P-Cc Ch-B-P-Cc Ch-B-KF-P Ch-M-KF-P Ch-M-A-P	[24] Ch-B-KF-Cc Ch-KF-P-Cc Ch-M-KF-P		[25] Ch-B-KF-Cc Ch-M-KF-Cc Ch-M-P-Cc Ch-M-A-P	[26] Ch-B-KF-Cc Ch-M-KF-Cc Ch-M-A-Cc

donite. Reaction V is necessary because of the experimentally demonstrated existence of reaction VI.

Zen (1961) has investigated the effect of changes in μ_{CO_2} and has postulated the reactions

(A) heulandite⇌aluminous silicate+calcite and
(B) laumontite⇌aluminous silicate+calcite
If prehnite is present, a third reaction is necessary
(C) prehnite⇌aluminous silicate+calcite

Zen (1961) has also pointed out that the slope of reaction (B) must be steeper than that of reaction (A). Similarly, the slope of reaction (C) must be steeper than that of reaction (B).

Reactions III, (A), (B) and reactions IV, (B), (C) intersect each in an isobaric-isothermal invariant point; that is, stable branches of reactions III and IV do not extend to the right of the "zeolite fence" A–B–C. Reactions involving celadonite (I, II, V and VI) are not affected by reactions (A), (B) and (C) and their stable branches therefore extend across the "zeolite fence." All zeolite assemblages lie to the left (low μ_{CO_2}) of the "zeolite fence" and all A+Cc assemblages lie to the right of it (high μ_{CO_2}).

From the relative positions of reactions, I, II, III, IV, V, VI, A, B and C it is possible to derive a complete isothermal-isobaric μ_{H_2O}-μ_{CO_2} diagram. A number of additional reactions become necessary for topological reasons:

(D) heulandite+potash feldspar⇌muscovite+calcite
(E) laumontite+potash feldspar⇌muscovite+calcite
(F) prehnite+potash feldspar⇌muscovite+calcite
(G) celadonite+heulandite⇌chlorite+muscovite+calcite
(H) celadonite+heulandite⇌chlorite+potash feldspar+calcite
(I) celadonite+laumontite⇌chlorite+potash feldspar+calcite
(J) celadonite+prehnite⇌chlorite+potash feldspar+calcite
(K) biotite+prehnite⇌celadonite+chlorite+calcite
(L) biotite+prehnite⇌chlorite+potash feldspar+calcite

The locations of these additional reactions are completely defined within the μ_{H_2O}-μ_{CO_2} diagram by the correlative requirements that a particular phase boundary must represent a single reaction only and that mineral assemblage in adjacent μ_{H_2O}-μ_{CO_2} fields differ by a single reaction only.

Figure 22 shows the complete graphical analysis and gives all possible mineral assemblages for each of the 26 different μ_{H_2O}-μ_{CO_2} fields. Many possible assemblages have not been found because of the wide range of bulk compositions required.

There are no discrepancies between observed assemblages, experimental data and Fig. 22. This is not to imply that this figure represents

the *only possible solution*, but does indicate that an arrangement similar is the probable solution. As mentioned earlier, adjustments in Fig. 21 will most certainly become necessary as more information becomes known about celadonite-bearing assemblages both from natural and synthetic studies.

It is also very important to realize that, because of the type of projection used, some of the reactions shown may take place not along a sharp curve but over a band of finite width. This is, as mentioned before, because participating phases do not necessarily have the same MgO/FeO or Fe_2O_3/Al_2O_3 ratios. There will be a band in the μ_{H_2O}-μ_{CO_2} plot for instance where celadonite+biotite+chlorite+muscovite may coexist in equilibrium over a range of μ_{H_2O} and μ_{CO_2} values with a different MgO/FeO and Fe_2O_3/Al_2O_3 ratio for each of the participating phases and so on.

Several other omissions in Fig. 22 deal with the Ch-A-Cc front face of the pyramid, particularly with respect to pumpellyite, which has been found to coexist with celadonite (Prostka, 1963). However, an extension to include such assemblages is not considered to be useful at this time because of the lack of relevant information.

Summary

Chemical data on celadonite are meager and hard to obtain. Since celadonite is generally associated with some other phyllosilicate, separation is often impossible. Only when celadonite occurs by itself in amygdule fillings can sufficiently pure material be obtained for chemical analysis. Chemical evidence accumulated thus far indicates that the occupancy of the tetrahedral layer in celadonite varies between Si_4 and $Si_{3.70}Al_{0.30}$ per 12 oxygens. Glauconites are distinguished from celadonites principally by their higher content of tetrahedral aluminum. In the octahedral layer the $MgFe^{3+}$-end member predominates, although some ferrous iron proxies for magnesium and a considerable amount of aluminum can replace the ferric iron. Octahedral occupancy is always close to two.

Infrared absorption spectra of celadonites differ significantly from those of glauconites, which show patterns more closely related to those of muscovites. *X*-ray data indicate that all natural and synthetic celadonites investigated so far belong to the 1M type.

Thus far celadonite has been reported mostly from altered or weakly metamorphosed volcanic rocks where it is closely associated with the zeolites—clinoptilolite, heulandite, and laumontite—and prehnite. It is also commonly accompanied by clay minerals, such as montmorillonite. The association with zeolites indicates that conditions required for the formation of zeolites (high μ_{H_2O}-low μ_{CO_2} environments) also favor the formation of celadonites.

The upper stability limit of the $MgFe^{3+}$-celadonite at a water pressure of 2,000 bars lies between about 400° and 440° C. depending upon the magnitude of f_{O_2}. This celadonite is stable under very reducing conditions (magnetite+iron buffer). With increasing oxygen fugacity its *b* and *c* cell dimensions decrease, its mean refractive index increases, and its stability field expands. High temperature breakdown products include iron-biotite and iron sanidine. Preliminary data on the stability of iron-sanidine as a function of f_{O_2} and T agree well with and extend published data on ferrisanidine and ferriannite.

Data on the upper stability limit of celadonite are not very useful in interpreting natural celadonite occurrences, since the temperatures far exceed estimates of the zeolite and prehnite-pumpellyite facies. Also, the reactions studied in the synthetic system do not correspond to any reactions inferred from natural assemblages. Natural celadonites must disappear during progressive metamorphism long before celadonite itself becomes unstable. This is accomplished most probably by interaction of celadonite with an aluminous silicate, such as montmorillonite. It is possible to postulate a series of steps and to construct a preliminary μ_{H_2O}-μ_{CO_2} grid, based on reactions inferred from natural assemblages and on the reaction studied in the synthetic system. Such a grid can be a valuable aid in studying assemblages from the lower grades of metamorphism, involving celadonite and zeolites or their compositional equivalents.

References

Bayramgil, O., Th. Hügi, and W. Nowacki (1952) Über ein Seladonitvorkommen im Gebiete von Zonguldak (Turkei). *Schweiz. Mineral. Petrog. Mitt.* **32,** 243–250.

Blake, R. L. (1958) A study of the iron silicate minerals in iron-formations of the Lake Superior region, with emphasis on the Cuyuna district. Ph.D. diss., Univ. Minnesota, Minneapolis, Minnesota.

Burst, J. F. (1958) Mineral heterogeneity of "glauconite" pellets: *Am. Mineral.* **43,** 481–487.

Chayes, F. (1955) Potash feldspar as a by-product of the biotite-chlorite transformation. *Jour. Geol.* **63,** 75–82.

Coombs, D. S. (1954) The nature and alteration of some Triassic sediments from Southland, New Zealand. *Trans. Roy. Soc. New Zealand,* **82,** 65–109.

——— (1960) Lower grade mineral facies in New Zealand. *Rept. Intl. Geol. Congress, XXI Sess., Part* **XIII,** 339–351.

——— (1961) Some recent work on the lower grades of metamorphism. *Austral. Jour. Sci.* **24,** 203–215.

———, A. J. Ellis, W. S. Fyfe and A. M. Taylor (1959) The zeolite facies, with comments on the interpretation of hydrothermal syntheses: *Geochim. Cosmochim. Acta,* **17,** 53–107.

Deer, W. A., R. A. Howie and J. Zussman (1962) *Rock forming Silicates, Vol. 3, Sheet silicates.* London.

De Lisle (1788) *Rome, Cristallographie, ou Description des formes propres a tous les corps du Regne mineral,* **2,** Paris.

DICKINSON, W. R. (1962) Metasomatic quartz kerotophyre in central Oregon. *Am. Jour. Sci.* **260,** 249–266.

ERNST, W. G. (1960) The stability relations of magnesioriebeckite. *Geochim Cosmochim. Acta,* **19,** 10–40.

——— (1962) Synthesis, stability relations, and occurrence of riebeckite, and reibeckite-arkvedsonte solid solution. *Jour. Geol.* **70,** 689–736.

EUGSTER, H. P. (1957) Heterogeneous reactions involving oxidation and reduction at high pressures and temperatures. *Jour. Chem. Physics,* **26,** 1760.

——— AND D. R. WONES (1962) Stability relations of the ferruginous biotite, annite. *Jour. Petrology,* **3,** 82–125.

FARMER, V. C. (1958) The infra-red spectra of talc, saponite, and hectorite. *Mineral Mag.* **31,** 829–845.

FISKE, R. S. (1960) Stratigraphy and structure of lower and middle Tertiary rocks, Mt. Rainier National Park, Washington: PhD thesis, The Johns Hopkins Univ., Baltimore, Maryland.

FISHER, R. V. (1963) Clinoptilolite tuff from the John Day formation, Eastern Oregon. *The Ore Bin,* **24,** 197–203.

FOSTER, M. D. (1956) Correlation of dioctahedral potassium micas on the basis of their charge relations. *U. S. Geol. Surv. Bull.* **1036-D,** 57–67.

——— (1960) Layer charge relations in the dioctahedral and trioctahedral micas. *Am. Mineral.* **45,** 383–398.

———, H. P. EUGSTER AND D. R. WONES (1963) The atomic ratios of natural ferruginous biotites, with reference to "The stability of the ferruginous biotite, annite (a discussion). *Jour. Petrology,* **4,** 302–306.

GLOCKER, E. F. (1847) *Generum et Specierum Mineralium secundum Ordires Naturales diagestorum Synopsis. Halle.*

GOGISHVILI, V. G. (1959) Celadonite from the surroundings of Tbilisi. *Geol. Sbornik Kavkaz. Inst. Mineral. Syr'ya,* **1,** 134–136.

GRUNER, J. W. (1935) The structural relationship of glauconite and mica. *Am. Mineral.* **20,** 699–714.

HAY, R. L. (1962) Origin and diagenetic alteration of the lower part of the John Day formation near Mitchell, Oregon. *Buddington Vol. Geol. Soc. Am.,* 191–216.

——— (1963) Stratigraphy and zeolitic diagenesis of the John Day Formation of Oregon: *Univ. Calif. Publ. Geol. Sci.* **42,** 199–262.

HEDDLE, M. F. (1879) The minerals of Scotland: Celadonite. *Trans Roy. Soc. Edinburgh,* **29,** 101–104.

HENDRICKS, S. B. AND C. S. ROSS (1941) Chemical composition and genesis of glauconite and celadonite. *Am. Mineral,* **26,** 683–708.

HEY, M. H. (1932) Studies on the zeolites. Part II: Thomsonite (including Faroelite) and gonnardite. *Mineral Mag.* **23,** 51–125.

HOWER, J. (1961) Some factors concerning the nature and origin of glauconite. *Am. Mineral.* **47,** 886–896.

HUTTON, C. O. AND F. T. SEELYE (1941) Composition and properties of some New Zealand glauconites. *Am. Mineral.* **26,** 595–604.

KARDYMOWICZ, I. (1960) Celadonite from Barcza in the Swietokrzyskie Mountains (Central Poland). *Kwart. Geol.* **4,** 609–616.

KVALVASER, I. A. (1953) On celadonite from Karadagh in the Crimea. *Miner. Sbornik, Lvov Geol. Soc.,* **7,** 223–226.

KOENIG, G. A. (1912) New observations in chemistry and mineralogy. *Jour. Phila. Acad. Nat. Sci.* **15,** 407–426.

LACROIX, M. A. (1916) Sur le mineral colorant le plasma de Madagascar et sur la celadonite. *Soc. franc. Mineral. Bull.* **39,** 90–95.

LAMBERT, R. ST. J. (1959) The mineralogy and metamorphism of the Moine schists of the Morar and Knoydart districts of Inverness-shire. *Proc. Roy. Soc. Edinburgh,* **63,** 553.

LAZARENKO, E. K. (1956) Celadonites from the basalts of Volhyria. *Miner. Sbornik, Lvov Geol. Soc.* **10,** 352–356.

LEVI, M. G. (1914) Sulle celadoniti di alcune localita venet: *Revista Mineral Crist. Italiana,* **43,** 74.

LIESE, H. C. (1963) Tetrahedrally coordinated aluminum in some natural biotites: An infrared absorption analysis. *Am. Mineral.* **48,** 970–1023.

LYON, R. J. P. (1963) Evaluation of infrared spectrophotometry for compositional analysis of lunar and planetary soils. *NASA Tech. Note* **D-1871.**

——— AND W. W. TUDDENHAM (1960) Determination of tetrahedral aluminum in mica by infrared absorption. *Nature,* **185,** 374–375.

MAEGDEFRAU, E. AND J. HOFMANN (1937) Glimmerartige Mineralien als Tonsubtanzen. *Zeit Krist.* **A98,** 31–59.

MALKOVA, K. A. (1956) Celadonite from Bug Region. *Miner. Sbornik, Lvov Geol. Soc.* **10,** 305–318.

OWENS, J. P. AND J. P. MINARD (1960) Some characteristics of glauconite from the coastal plain formations of New Jersey. *U. S. Geol. Surv. Prof. Paper* **400,** B430–B432.

PROSTKA, H. (1963) The geology of the Sparta Quad., Oregon: Ph.D. thesis, The Johns Hopkins Univ., Baltimore, Maryland.

RADOSLOVICH, E. W. (1963a) The cell dimensions and symmetry of layer lattice silicates. IV. Interatomic forces. *Am. Mineral.* **48,** 76–99.

——— (1963b) The cell dimensions and symmetry of layer lattice silicates. V. Composition limits. *Am. Mineral.* **48,** 348–367.

ROEDDER, E. (1952) A reconnaissance of liquidus relations in the system $K_2O \cdot 2SiO_2$-FeO-SiO_2. *Am. Jour. Sci., Bowen vol.,* 435–456.

ROSS, C. S. (1958) Welded tuff from deep-well cores from Clinch County, Georgia. *Am. Mineral.* **43,** 537–545.

SCHAIRER, J. F. AND N. L. BOWEN (1955) The system K_2O-Al_2O_3-SiO_2. *Am. Jour. Sci.* **253,** 681–746.

SCHALLER, W. T. (1950) An intepretation of the composition of high-silica sericites. *Mineral Mag.* **29,** 406–415.

SCHERILLO, A. (1938) Celadonite in an eruptive rock in Erythrea. *Period. Mineral Roma,* **9,** 253–264.

SCHÜLLER, A. AND E. WOHLMANN (1951) Über Seladonit und seine systematische Stellung. *Neues Jahrb. Mineral.* **82,** 111–120.

SHAW, H. R. (1963) Hydrogen-water vapor mixtures: control of hydrothermal atmospheres by hydrogen osmosis. *Science,* **139,** 1220–1222.

SMOLIKOWAKI, K. (1936) On skolicie, a new mineral of the glauconite group. *Arch. Mineral.* **12,** 144–178.

STEINFINK, H. (1962) Crystal structure of a trioctahedral mica: phlogopite. *Am. Mineral.* **47,** 886–896.

SUDO, T. (1951) Mineralogy of green tuff-greccia near Schiroishi-machi, Miyagi pref. *Jour. Geol. Soc. Japan* **57,** 842–858.

——— (1953) *Nendo-Koubusto* (Clay Mineralogy), Tokyo.

THOMPSON, J. B. (1957) The graphical analysis of mineral assemblages in pelitic schists. *Am. Mineral.* **42,** 842–858.

TUDDENHAM, W. W. AND R. J. P. LYON (1959) Relation of infrared spectra and chemical analysis for some chlorites and related minerals. *Anal. Chem.* **31,** 377–380.

TYLER, S. A. AND S. W. BAILEY (1961) Secondary glauconite in the Biwabic Iron-formation of Minnesota. *Econ. Geol.* **56,** 1030–1044.

WELLS, R. C. (1937) Analyses of rocks and minerals from the laboratory of the U. S. Geol. Survey. *U. S. Geol. Survey. Bull.* **878.**

WISE, W. S. (1961) The geology and mineralogy of the Wind River area, Washington, and the stability relations of celadonite. Ph.D. thesis, The Johns Hopkins Univ., Baltimore, Maryland.

WONES, D. R. (1958) The phlogopite-annite join. *Carn. Inst. Wash. Yearbook* **57,** 194–195.

——— (1963) Phase equilibria of "ferriannite," $KFe_3^{+2}Fe^{+3}Si_3O_{10}(OH)_2$: *Am. Jour. Sci.* **261,** 581–596.

——— AND D. E. APPLEMAN (1961) X-ray crystallography and optical properties of synthetic monoclinic $KFeSi_3O_8$, Iron sanidine. *U. S. Geol. Surv. Prof. Paper* **424,** C309–C310.

——— AND D. E. APPLEMAN (1963) Properties of synthetic triclinic $KFeSi_3O_8$, Iron microcline, with some observations on the iron-microcline=iron-sanidine transition. *Jour. Petrology,* **4,** 131–137.

YODER, H. S. AND H. P. EUGSTER (1954) Phlogopite synthesis and stability range. *Geochim. Cosmochim. Acta,* **6,** 157–185.

——— (1955) Synthetic and natural muscovites. *Geochim. Cosmochim. Acta,* **8,** 225–280.

ZEN, EAN. (1960) Metamorphism of lower Paleozoic rocks of the Taconic range in Vermont. *Am. Mineral.* **45,** 129–175.

——— (1961) The zeolite facies: an interpretation. *Am. Jour. Sci.* **259,** 401–409.

ZUSSMAN, J. (1955) The crystal structure of an actinolite. *Acta Cryst.* **8,** 301–308.

Manuscript received, January 2, 1964; accepted for publication, March 16, 1964.